TITLE: Thermo-sensitive condensation of SUF4 tunes flowering time in *Arabidopsis thaliana*

AUTHORS: Heather M. Meyer[1*], Takashi Hotta[2,3], Andrey Malkovskiy[1], Yixian Zheng[2], and David W. Ehrhardt[1*]

AFFILIATIONS: 1. Department of Plant Biology, Carnegie Institution for Science, Stanford, CA 94305, USA. **2.** Department of Embryology, Carnegie Institution for Science, 3520 San Martin Dr. Baltimore, MD 21218, USA. **3.** Department of Cell and Developmental Biology, University of Michigan, Ann Arbor, 109 Zina Pitcher Pl. Ann Arbor MI 48109, USA * Corresponding authors: Heather M. Meyer:hmeyer@ciw.edu, David W. Ehrhardt: ehrhardt@stanford.edu

KEYWORDS: *Arabidopsis thaliana*, Flowering-time proteins, biomolecular condensates, tuning protein condensation

ABSTRACT (271 words): Intrinsically disordered proteins (IDP) lack stable tertiary structures, which allows them to change conformation and function under different physicochemical conditions. This may be highly advantageous for plants, which often use changes in their environment to trigger developmental events. For instance, some plants use exposure to winter temperatures as a cue to initiate flowering the following spring. Many of the genes involved in temperature-dependent flowering have been extensively studied in *Arabidopsis*, yet how plants perceive temperature changes is poorly understood. Here, we explore the role of temperature-sensitive phase separation of the IDP and flowering-time regulator, SUPPRESSOR OF FRIGIDA 4 (SUF4), in modulating flowering time. SUF4 has a well-defined role in regulating temperature-dependent flowering time by activating the master floral suppressor *FLOWERING LOCUS C (FLC)*. We show that in plant nuclei, SUF4 is a temperature-sensitive protein that assembles into biomolecular condensates in warm temperatures (20°C). When temperatures cool (4°C), SUF4 nuclear condensates disassemble, causing SUF4 to disperse within the nucleoplasm. Additionally, we demonstrate that the number of SUF4 condensates quantitatively correlates with flowering time. Progressive alterations to the amino acid composition of SUF4's disordered region cause likewise progressive changes in temperature-dependent condensation both *in vitro* and *in vivo*, *FLC* transcription, and the onset of flowering. We also observe that SUF4 condensates coincide with the accumulation of other key flowering-time proteins (FRIGIDA and ELF7). These findings indicate that condensation of SUF4 likely plays a pivotal role in promoting flowering, possibly by concentrating and stabilizing the regulatory factors needed for the transcriptional activation of *FLC* through temperature-dependent phase separation. This research suggests that in plants, IDPs can sense environmental cues and regulate critical developmental processes.

INTRODUCTION:

The survival of all living organisms depends on their ability to reproduce. For plants, reproductive success relies heavily on the onset of flowering, a phenological feature that is influenced by changes in seasons. Many plant species, including winter crops, have evolved to use long exposure to winter temperatures (e.g. vernalization) as a cue to flower in the following spring. Temperature-induced development plays a crucial role in the long-term reproductive success and yield of plants, enabling them to synchronize their flowering with seasonal pollinators and set seed during favorable climatic conditions. Thus, as climate change drives new spatial and seasonal temperature trends, it is increasingly important to understand how plants physically sense and integrate thermal shifts.

In the model plant, *Arabidopsis thaliana*, temperature-dependent flowering is modulated by the epigenetic silencing of the *FLOWERING LOCUS C* (*FLC*). *FLC* encodes for a MADS-box transcription factor that functions to repress flowering by silencing floral-inducing genes including *FT* and *SOC1* (*1–3*). In warm temperatures, SUPPRESSOR OF FRIGIDA 4 (SUF4), FRIGIDA (FRI) and FRI-associated proteins transcriptionally activate *FLC* by recruiting chromatin modifiers, such as members of the PAF1 complex, which methylate histone h3 lysine 4 (H3K4me3) at *FLC*'s transcriptional start site (*3*). Conversely, exposure to cold temperatures promote antisense long non-coding RNAs and a second set of chromatin remodelers belonging to the POLYCOMB REPRESSIVE COMPLEX 2 (PRC2) to epigenetically silence *FLC*, ultimately priming plants to flower the following spring (*4*, *5*). While many elements of the genetic and epigenetic regulation of temperature-dependent flowering are well established, the mechanisms by which plants sense and transduce thermal changes to elicit these responses remains a mystery.

Intrinsically disordered proteins (IDPs) have been proposed to function as environmental sensors and signal transducers in a variety of species (*6*). Unlike canonical proteins that fold into relatively stable structures with constrained conformational changes when exposed to different stimuli and physiological environments, IDPs possess low sequence complexity and a greatly reduced ability to form stable tertiary structures. This inherent flexibility allows them to more freely change their conformation and function under varying physical and solution conditions. For instance, many IDPs undergo phase transitions into liquid-like protein droplets or viscoelastic hydrogels, enabling the quick concentration, formation and/or stabilization of higher order complexes in response to environmental changes (*7*, *8*). In recent years, an intriguing hypothesis has emerged, suggesting that environmentally-induced phase transitions may have evolved as a mechanism for cells and organisms to sense and transduce environmental information (*7*). Nevertheless, testing this hypothesis remains challenging, as it is difficult to assess the functional contributions of IDP phase transitions compared to other possible functions independent of phase change behavior.

Here, we leverage the *FLC* flowering time system as a genetic model to explore the role of IDP phase separation in sensing and transducing environmental cues. Several *FLC* transcriptional regulators contain intrinsically disordered regions (IDRs), with evidence of some regulators forming nuclear condensates (*3*, *9–12*). Specifically, we examined whether the flowering-time determinant and disordered protein SUF4 uses

temperature-dependent phase separation to regulate the onset of flowering time. SUF4 makes an excellent candidate for untangling the relationship between protein phase separation behavior and plant temperature sensing because it has a well-defined genetic and molecular role in temperature-dependent flowering by acting to transcriptionally regulate *FLC* under warm temperature conditions. Furthermore, it exhibits structural and biochemical similarities to BuGZ, a mammalian IDP that is proline-rich and undergoes temperature-dependent phase separation under *in vitro* conditions (*13–15*).

Using confocal microscopy, genetics and biochemistry, we have discovered that SUF4 is a temperature-sensitive protein that phase separates *in vitro* to form proteinaceous droplets and *in planta* to promote the formation of nuclear condensates. Under warm temperatures (20°C), SUF4 dynamically assembles into nuclear condensates, where it co-localizes with major flowering-time regulators, such as FRIDIGA (FRI) and the PAF1-complex member, EARLY FLOWERING 7 (ELF7). In contrast, nuclear condensates fail to form at low temperatures (4°C), resulting in SUF4 being diffuse within the nucleoplasm. Moreover, through the use of targeted mutagenesis, we have discovered that SUF4's disordered region is important for both nuclear condensate formation and flowering time; plants expressing SUF4 variants with aromatic/hydrophobic-to-hydrophilic substitutions in their disordered region display predictable changes in condensate formation, *FLC* transcript levels, and flowering-time responses. Our results support the hypothesis that SUF4 regulates flowering time by using temperature-dependent phase separation to concentrate and/or stabilize regulatory factors needed for the transcriptional activation of *FLC.*

RESULTS:

SUF4 forms nuclear condensates *in planta.*

The formation of biomolecular condensates is exquisitely sensitive to changes in the physicochemical properties of their environment (*7*). To test if SUF4 can form condensates in response to changes in temperature, we engineered a monomeric fluorescent mEGFP-SUF4 fusion protein expressed from the putative *SUF4* native promoter and 3' UTR (pSUF4::mEGFP-SUF4). Then, we introduced this construct into *suf4*(*FRI*) mutant plants, which displays an early flowering phenotype compared to the wild type (Col(FRI), Supplemental Fig. 1A and 1B) and determined if the engineered transgene rescued *SUF4* function. In *Arabidopsis*, the onset of flowering coincides with the cessation of rosette leaf production. Therefore, counting the number of rosette leaves provides a quantitative method for evaluating flowering time. Using this leaf counting assay, we identified several transgenic lines that rescued both the early flowering phenotype of the null mutant and the transcriptional activity of *SUF4* as measured by the transcripts level of its downstream target *FLC* (Supplemental Fig. 1A and 1B), suggesting that the *SUF4* transgene is fully functional and expressed at adequate levels. We picked one of these lines to perform all subsequent analyses regarding SUF4.

To assess the subcellular behavior of SUF4 at room temperature within living plant cells, we imaged live cells using confocal microscopy. In both the shoot and the root, we observed SUF4 to exhibit a diffuse localization pattern within the nucleoplasm and accumulate in nuclear foci reminiscent of biomolecular condensates (Fig. 1A, Supplemental Fig. 2). Additionally, we found that SUF4 localized in the nucleolar cavity, an elusive membrane-less compartment that forms within the nucleolus (Supplemental

Fig. 2). The nucleolar cavity is a thermo-responsive structure in plant cells that exchanges its contents with the nucleus (*16–18*). However, we directed our analysis toward the function of the nucleoplasmic foci outside of the nucleoli where most genes, such as *FLC*, are transcribed (*19*, *20*).

If SUF4 condensates function as thermosensors, their formation should exhibit temperature sensitivity across a physiologically relevant temperature range *in vivo*. To test this, we subjected SUF4 rescue plants to a 24-hour cold treatment at 4°C and then live imaged epidermal and cortical cells in the division and growth zones of primary roots as the plants rewarmed to 20°C. At the beginning of rewarming, mEGFP-SUF4 appeared diffuse and no condensates were detected (Fig. 1A and 1B). As plants began to warm up, SUF4 signal progressively partitioned into nuclear condensates, with condensates forming within seconds to minutes once exposed to room temperature conditions. To ensure that these changes were temperature-induced, we also imaged plants over the same time course under constant 20˚C (Fig. 1B). Although some condensates showed evidence of forming and dissipating over the time scale of observation (<10mins), a portion of SUF4 always remained partitioned in condensates. Together, our results suggest that SUF4 is a temperature-sensitive protein that assembles into biomolecular condensates in warm temperatures and remains diffuse in the nucleoplasm in cold temperatures.

SUF4 phase separates *in vitro*.

SUF4 is orthologous to the animal protein BuGZ (Supplemental Fig. 3), an IDP initially found to undergo temperature-dependent phase separation *in vitro* and regulate spindle assembly *in vivo* (*13–15*). Therefore, to assess the potential for SUF4 to undergo phase separation independently of any plant cell factors, we expressed and purified 6xHis-mVenus-SUF4 (isoform 1, WT) from SF9 insect cells. Using both fluorescence and DIC microscopy, we observed that 6xHis-mVenus-SUF4 underwent phase separation at high temperatures (25μM at 37˚C) and remained miscible at low temperatures (25μM at 4˚C) when suspended in physiologically relevant buffers (Fig. 1C, see methods). These results suggest that, similar to BuGZ, SUF4 is a phase-separating protein displaying low critical solution temperature (LCST) behavior. To investigate further the phase behavior of SUF4, we conducted a turbidity assay to determine the thermal setpoint required for SUF4's condensation. We found that 25μM of 6xHis-mVenus-SUF4 was fully miscible between 4-10˚C but became increasingly turbid as temperatures gradually rose to 30˚C (Fig. 1D). Additionally, in line with other phase-separating proteins, SUF4's phase transition is concentration-dependent, with lower concentrations of SUF4 requiring higher temperature regimes to undergo phase separation (Fig. 1D). These results indicate that, similar to BuGZ, SUF4 is a temperature-sensitive protein that undergoes LCST phase separation *in vitro*.

SUF4's disordered region drives nuclear condensate formation *in vitro* and *in planta.*

IDP phase separation is driven by multivalent interactions, such as those facilitated by aromatic/hydrophobic residues like tyrosine and phenylalanine. Moreover, these same residues are required for *in vitro* condensation of SUF4's ortholog, BuGZ (*14*). Despite being a proline-rich protein, SUF4 contains a total of 14 regularly spaced tyrosine and

phenylalanine residues within its disordered region, with two of these residues falling in putative splice sites (Supplemental Fig. 3). To test if aromatic/hydrophobic residues in SUF4's disorder region promote its temperature-dependent condensation, we created a SUF4 variant, termed 12S SUF4, in which we substituted 12 non-splice-interfering tyrosine and phenylalanine residues with serine and asked if this variant had a different phase separation thermal setpoint *in vitro*. We found 12S SUF4 had a large shift in its thermosensitive capabilities to phase separate, such that 25μM of purified 12S SUF4 now required temperatures nearing 50˚C to begin phase separating as opposed to 20˚C for the native protein (fig. 1D). These results suggest that changing SUF4's aromatic/hydrophobic patterning is sufficient to disrupt condensate formation *in vitro* by increasing the thermal set point at which SUF4 can phase separate.

To test if changes in SUF4 aromatic/hydrophobic patterning also influenced condensate formation *in vivo*, we generated the same 12 mutations in the mEGFP-SUF4 fusion protein expressed over a chromosomal null locus (pSUF4::mEGFP-12S SUF4). Similar to our observations *in vitro,* we found that 12S SUF4 exhibited a severe reduction in condensate formation *in vivo*. On average, 12S SUF4 plants formed 0-1 nuclear condensates per nucleus in root epidermal and cortical nuclei at 20˚C, as compared to 4-5 per nucleus formed in rescue SUF4 (Fig. 2A and 2B nuclei observed: 12S SUF4 n= 27, rescue SUF4 n=32). These results suggest that the altered coacervation properties of 12S SUF4 are maintained in the complex environment of the living cell.

Next, we investigated if SUF4 uses phase separation as a means to regulate flowering time. As a first step in testing this hypothesis, we asked if 12S SUF4 variant plants displayed a phenotypic difference in its response as compared to the rescue SUF4 plants. Using a leaf counting assay, we found that 12S SUF4 plants transitioned to flowering much sooner, producing significantly fewer rosette leaves before flowering (Short Day (SD): 60 leaves (n=19), Long Day (LD): 35 leaves (n=30)) as compared to SUF4 rescue plants (SD: 93 leaves (n=34), LD: 71 leaves (n=29)), but significantly more so than the *suf4* null mutant (SD: 45 leaves (n=22), LD: 26 leaves (n=31)) (Fig. 2D and 2E, Supplemental Fig. 4). Previous research has shown that high levels of *FLC* must be produced for the suppression of flowering time. We therefore asked if the flowering time phenotype caused by the 12S mutant protein was correlated with a reduction in *FLC* transcripts. We found plants expressing the 12S variant to produce approximately 18-fold fewer *FLC* transcripts than our SUF4 rescue lines but 2-fold more than *suf4* null mutants (Fig. 2E). Thus, although *FLC* still undergoes some transcription in the 12S SUF4 variant, the mutations that caused disruption of SUF4 temperature-sensitive condensation greatly accelerated the onset of flowering.

Tuning SUF4 phase behavior corresponds to changes in flowering time outcomes

Previous work from Jiang et al (2015) has shown that the *in vitro* phase behavior of SUF4's ortholog, BuGZ, may be tuned by incrementally decreasing the number of combined phenylalanine and tyrosine to serine substitutions (*14*). This finding, paired with the correlation between SUF4 phase separation and flowering time, prompted us to further assess if SUF4's phase change properties themselves were critical for dictating different flowering time outcomes. We reasoned that if so, substituting a smaller number of the phenylalanine and tyrosine residues should lead to a scalable intermediate phase separation phenotype and proportionally tune flowering time outcomes via decreasing the

transcriptional levels of *FLC*. To test this prediction, we created an intermediate SUF4 variant that only had 5 combined tyrosine and phenylalanine to serine substitutions termed, 5S SUF4, and assessed its phase separating thermal setpoint *in vitro*. Consistent with what had been observed for BuGZ, we found purified 5S SUF4 to have a thermal shift that ranges between the phase change of rescue SUF4 and 12S SUF4 *in vitro* (Fig. 1D; 25μM showed a steep phase transition at 40˚ C instead of 20˚C like rescue SUF4 and 50˚C like 12S SUF4).

To test the function of the 5S SUF4 variant *in vivo*, we introduced it into *suf4* null mutant plants and asked whether these plants exhibited intermediate phenotypes relating to SUF4 phase separation, *FLC* transcriptional output, and flowering time. Remarkably, we found 5S SUF4 plants to display an intermediate condensate phenotype *in vivo*, in which they formed significantly fewer nuclear condensates in root epidermal and cortical cells than rescue SUF4 but more than 12S SUF4 (Fig. 2A and 2B; rescue SUF4:4-5, 5S SUF4:2-3, 12S SUF4:0-1). Moreover, 5S SUF4 plants exhibited *FLC* transcript levels and flowering time responses that both fell between rescue SUF4 and 12S (Fig. 2C, 2D, 2E, Supplemental Fig. 4; rescue SUF4 produced 20-fold/ SD:93 leaves (n=34) and LD: 71 leaves (n=29), 5S SUF4: 10-fold/ SD: 70 leaves (n=18) and LD: 43 leaves (n=39), 12S SUF4 3-fold/ SD: 60 leaves (n=20) and LD: 35 leaves (n=30)). These results suggest that tuning the LCST behavior of SUF4 is sufficient to predictably change the onset of flowering through modulating transcript levels of *FLC*.

SUF4's exchange dynamics scale with changes in LCST behavior

Biomolecular condensates may assume a broad range of material properties, spanning liquid-, gel-, or solid-like structures, with these respective properties often being hypothesized as being important for their biological function (*6*, *21–23*). Under *in vitro* conditions, purified and condensed SUF4 exhibited behavior consistent with a liquid, similar to its ortholog BuGZ. For example, *in vitro* condensates on glass assume a round outline, as expected at a liquid-liquid interface, and are rapidly and repeatedly reversible with temperature change (Fig. 1C, Supplemental Fig. 5). However, whether SUF4's material properties remain liquid-like during interactions with other biomolecules under native cellular conditions remains unknown. Previous research has suggested that the exchange dynamics of molecules within condensates are expected to correlate with their material state, with faster exchange rates in liquid-like condensates and slower rates in more solid-like structures. Thus, to investigate the exchange dynamics of SUF4 and whether these dynamics are affected in our SUF4 variants, we conducted fluorescence recovery after photobleaching (FRAP) experiments on rescue SUF4, 5S SUF4, and a hydrophobic variant termed 30I SUF4, which contains 30 alanine-to-isoleucine substitutions in its disordered region. We excluded the 12S SUF4 variant as it rarely formed condensates. FRAP was performed in a small region of approximately 1.094 microns^2, centered on a prominent mEGFP-SUF4 nuclear body in each cell assayed. Our findings revealed that changing the hydrophobicity of SUF4 greatly affected its FRAP dynamics. 30I SUF4 condensates did not reach their half recovery time within a 10-minute period, whereas both rescue SUF4 and 5S SUF4 rapidly reached their half recovery time within seconds (Fig 2F., rescue SUF4: t1/2=1.27 seconds, n=13; 5S SUF4 t1/2=0.85 seconds, n=12, 1-sided t-test $p<0.01$). Additionally, 30I SUF4 condensates exhibited a higher "immobile" fraction compared to SUF4 rescue and 5S SUF4, which both largely

recovered (30I SUF4 = 0.094 mobile fraction, SUF4 rescue = 0.85 mobile fraction, and 5S SUF4 = 0.76 mobile fraction; Fig 2F). Interestingly, despite 30I SUF4 having formed many condensates that were relatively slow to recover, we did not observe any rescue in plant phenotype concerning *FLC* transcription or flowering time (Fig. 2A-2E and Supplemental Fig. 4). Previous studies have suggested that the biophysical properties of some condensates must fall within a fluidic window, in which being overly solid or fluid-like can lead to a decrease in functionality (*23–28*). Therefore, in agreement with these findings, we propose that SUF4 needs to maintain a specific state of fluidity in order to function optimally.

A notable finding from our FRAP experiments is that the recovery curves of 5S SUF4 signal exhibited a lower R^2 value on average when fitted to a single exponential recovery model, along with a lower bleaching depth compared to those observed in our rescue lines (rescue SUF4 R^2 = .73, 5S SUF4 R^2 = .53). This observation prompted us to further investigate the behavior of condensates in this background. In doing so, we noticed that 5S SUF4 condensates appeared to display greater motility compared to rescue SUF4 condensates. An increase in particle motility could explain the reduced model fit as movement of condensates out of the focal plane would tend to reduce their brightness, thus affecting measurement of signal recovery kinetics. To quantify the perceived difference in motility, we measured the total distance traveled by each condensate during our FRAP analysis. On average, we found that 5S SUF4 condensates traveled significantly greater distances within the nucleoplasm compared to rescue SUF4 condensates (Supplemental Fig. 6, average distance of 1.802 microns for rescue SUF4 and 3.046 microns for 5S SUF4). These results indicate that 5S SUF4 condensates are less constrained in their positional behavior compared to their rescue SUF4 counterparts.

SUF4 colocalizes with FRI within nuclear condensates under room temperatures in cells recently derived from meristems

SUF4 has been shown previously to physically and genetically interact with FRIGIDA (FRI) and other members of the vernalization pathway, and this complex has been proposed to transcriptionally activate *FLC* (*3*, *29*). Therefore, to explore the possibility that SUF4 condensation might function to regulate *FLC* by concentrating flowering time proteins, we tested if there was an observable spatial relationship between SUF4 and FRI *in vivo*. We generated a fluorescently-labeled FRI fusion gene (FRI-mScarletI) that expresses from the native upstream sequence of FRI (pFRI) and transformed it into a mEGFP-SUF4 rescue line. Under room temperature conditions, we found FRI-mScarletI to exist in one of two distinct phase states within the nucleoplasm of root epidermal and cortical cells within the division and growth zones— either uncondensed and diffuse within the nucleoplasm or assembled into one-to-two apparent condensates (Fig 3A).

Next, we tested if FRI-mScarletI condensates colocalized with mEGFP-SUF4 condensates. To measure co-localization, we considered condensates to be colocalized if the centroids of spot-detected condensates were closer together than the radius of the kernel used to detect the SUF4 condensates (<250nm). Out of 56 FRI-mScarletI condensates analyzed, 38 of them co-localized with a SUF4 condensate (Fig. 3A and 3B; 68% co-localization, n=47 nuclei, distance threshold=0.3μm). To ask whether this degree of colocalization was specific to the vernalization complex and not likely due to chance

alone given the density of SUF4 nuclear condensates, we co-transformed the nuclear splicing speckle marker U2B”-mRFP into mEGFP-SUF4 rescue plants, a marker, like that for FRI, produces 1-2 bodies of larger size per nucleus. In the 18 nuclei examined, we found no instances of U2B" bodies co-localizing with SUF4 at room temperature conditions (0/19 U2B” speckles; Fig. 3A). These data demonstrate a remarkable degree of colocalization between SUF4 and FRI. Moreover, they suggest that the formation of FRI condensates under warm temperatures is not a random occurrence but rather selective for co-condensation with SUF4.

FRI has recently been demonstrated to have diminished physical interactions with SUF4, and accumulate into nuclear condensates when exposed to extended periods of low temperatures (*9–11*). Thus, to test the spatial relationship between SUF4 and FRI in the cold, we exposed mEGFP-SUF4 and FRI-mScarletI co-expressing plants to 4˚C for 24 hours, and imaged their root cells as the plants warmed up. Consistent with previous findings (*9–11*), we found FRI to form cold-induced nuclear condensates. However, unlike the case at room temperature (~21˚C), these condensates did not co-localize with SUF4. Instead, SUF4 condensates would sometimes appear where FRI condensates previously existed as the plant began to warm (observed in at least 7 nuclei; Fig 3C). These results suggest an antagonistic or independent relationship between cold-induced FRI condensates and SUF4. Additionally, they suggest that FRI undergoes cold-induced phase separation that is independent of *FLC* activation.

Given the established relationship between the spatiotemporal organization of proteins and their biological function, we investigated the root tissue types in which both warm- and cold-induced FRI condensation occurred. Under warm temperatures, we observed the presence of FRI condensates in the division and growth zones of a subset of emerging and young lateral roots but not in the primary roots (Nplants=8/29 lateral roots, Nplants=0/34 primary roots of 6-13 DAG). This was different to what occurred under cold temperatures, in which we found FRI condensing in all root types, including the primary roots (Supplemental Fig. 3A). Interestingly, the occurrence of warm-induced FRI condensates within a given lateral root cell was highly variable among lateral roots, with detectable FRI-mScarletI condensates found in anywhere from 30% to 94% of the epidermal and cortical cells within the growth zone (Supplemental Fig. 7). The seemingly stochastic patterns of nuclei containing FRI condensates among and within lateral meristems resemble the previously described phenomenon of transcriptional and translational "bursting," which has been associated with epigenetic and phenotypic diversity in response to environmental changes (*19*, *30*).

Previous research has highlighted the influence of plant tissue types on the state of auxin response factor (ARF) biomolecular condensates (*31*). The observation of co-condensation between SUF4 and FRI in lateral roots, while absent in primary roots of 6-13 days after germination plants, suggests the potential for a tissue-specific functional relationship between these proteins. If this is true, we might observe a tissue-specific change in mScarletI-FRI condensate behavior in response to changes in SUF4 condensation. To test this hypothesis, we introduced FRI-mScarlet into suf4 null, 12S SUF4, and 5S SUF4 variant plants. At room temperatures, we observed the formation of FRI-mScarletI condensates in about 10%-25% of primary roots of suf4 null and 12S SUF4 plants, respectively (Fig. 3D, Table. 1; suf4 4/41, 12S SUF4 4/5), but no FRI-mScarletI condensates were observed in the primary roots of rescue SUF4 (0/34) or 5S SUF4 lines

(0/19). FRI-mScarletI condensates were observed in a portion of lateral roots in all lines. Although the number of mGFP-SUF4 condensates varies among rescue SUF4 and 5S SUF4, both have the ability to form condensates, whereas 12S and *suf4*(*FRI*) do not. Thus, our data suggest that an inverse relationship exists between SUF4 and FRI condensates in the primary root. Furthermore, it suggests that FRI is capable of forming at least two distinct types of condensates that vary by tissue type: one type that collaboratively forms with SUF4, likely functioning to help establish *FLC* transcription in newly formed tissue, and another type where the proteins possibly act antagonistically.

Table 1. FRI-mscarletI condensate formation in different root types within SUF4 variants

Condensate formation	**Lateral**		**Primary**	
Genotype	Warm	Cold	Warm	Cold
FRI-mScarletI (*meGFP-SUF4*)	Yes (n=8/29 roots)	?	No (n=0/34 roots)	Yes
FRI-mScarletI (meGFP-5S SUF4)	Yes (n=2/6 roots)	?	No (n=0/19 roots)	Yes
FRI-mScarletI (meGFP-12S SUF4)	Yes (n=2/2 roots)	?	Yes (n=4/5 roots)	Yes
FRI-mScarletI (*suf4 null*)	Yes (n=5/22 roots)	?	Yes (n=4/41 roots)	Yes

SUF4 colocalizes in nuclear condensates with ELF7 under room temperatures

While FRI facilitates transcriptional activation of *FLC* by establishing a permissive chromatin environment, other mechanisms have been shown to be involved in the maintenance of *FLC* expression, such as transcriptional regulation associated with histone H3 lysine 4 (H3K4) modifications (*29*, *32*). In light of this, we sought to investigate whether SUF4 condensates might serve as a hub for multiple proteins involved in the transcriptional regulation of *FLC* by fluorescently tagging and expressing EARLY FLOWERING 7 (ELF7), a known member of the PAF1 complex. We introduced mTFP-ELF7 expressed from its own upstream sequence (pELFF7::mTFP-ELF7) into rescue lines expressing mEGFP-SUF4 and mEGFP-SUF4/FRI-mScarletI. ELF7 was specifically chosen due to its previous genetic interaction with SUF4 and its role in establishing H3K4 activation marks on *FLC*, as well as its physical co-localization with FRI in nuclear condensates under normal temperature conditions (*10*, *29*, *32*). Within both transgenic lines, we observed mTFP-ELF7 to be diffuse within the nucleoplasm of cortical and epidermal cells within the transition zone of both lateral and primary roots. In a subset of these cells, mTFP-ELF7 formed 1-2 prominent nuclear condensates and occasionally multiple smaller condensates (Fig. 3C).

As the introduction of mTFP-ELF7 did not appear to induce silencing, nor alter condensate behavior in either the rescue mEGFP-SUF4 or mEGFP-SUF4/FRI-mScarletI lines, we performed colocalization analysis using lines expressing all three transgenes (Fig. 3C). While mEGFP-SUF4 formed more condensates compared to ELF7 and FRI in nuclei analyzed (nSUF4condensates= 414, nELF7condensates= 53, nFRIcondensates= 34), the presence of an ELF7 condensate almost always coincided with a SUF4 condensate (47 out of 53 cases). Further, out of these 47 ELF7-SUF4-containing condensates, we observed the additional presence of a FRI condensate in 8 cases (17%).

These observations suggest that SUF4 assembles into condensates that house other members of the vernalization complex. Considering that SUF4 forms multiple condensates, and FRI and/or ELF7 only co-localize in 1-2 of these per nuclei, an interesting possibility is that these condensates may be specialized for *FLC* regulation prior to vernalization. The quantitative correlation between SUF4 condensation and flowering time, coupled with its ability to co-condense with both FRI and ELF7, supports the notion that SUF4 likely acts as a scaffold, hub, or part of a molecular address for the vernalization complex in regulating the transcriptional activity of *FLC* under different temperature conditions (Fig. 4).

DISCUSSION:

In this study, we have discovered that the IDP, SUF4, undergoes thermally-regulated condensation both *in vitro* and *in planta*. These findings, along with the demonstrated ability of SUF4 sequence alterations to progressively tune phase separation, *FLC* transcription, and predictable flowering time outcomes, and the evidence that SUF4 condenses with *FLC* transcriptional regulators under appropriate physiological conditions, provide strong support for the hypothesis that SUF4 phase separation serves as a physical mechanism for plant temperature perception. Our work emphasizes the biological importance of protein phase separation in a multicellular organism by establishing links between environmentally-sensitive phase separation, gene expression, development and physiology.

Plant cells require an ability to filter out noise and interpret meaningful signals from their environment to make developmental decisions. The conformational promiscuity and multivalency of IDPs enables them to engage in a variety of specific yet transient interactions under defined environmental conditions. IDPs are enriched within plant proteomes, with many participating in plant regulatory pathways and as integrators of environmental inputs (*33*–*35*). The phase separation states of such IDPs and client proteins could serve as an effective mechanism for distinguishing real signals from noise within plant cells, thereby enabling more efficient and effective developmental outcomes. Plants, along with other organisms, use epigenetic factors, such as changes in chromatin/histone state, signaling pathways, and RNA modifications to promote environmental-driven developmental changes. However, these changes often require integration over a significant period of time in order to induce a physiologically-relevant response. Pairing IDP sensing with slower-acting epigenetic mechanisms may allow plants to better distinguish genuine signals from noise by facilitating the promotion or maintenance of molecular memory under persistent environmental cues. In the case of SUF4, we found that changes in temperature cause it to phase transition between condensed and uncondensed forms. Moreover, manipulating the aromatic/hydrophobic properties of SUF4 proved to be sufficient to modulate its material characteristics and tune the onset of flowering. Given SUF4's known interaction with *FLC*-related chromatin remodelers and our cell biological evidence that they co-condense with SUF4 *in vivo*, these findings suggest that SUF4 condensates may serve as thermosensors by associating with epigenetic factors to modulate *FLC* transcription.

Extensive investigations have shed light on the intricate regulation of flowering time in *Arabidopsis*, with a specific emphasis on the transcriptional modulation of *FLC* (*36*). Among the key players in this regulatory network is FRI, an interacting partner of SUF4

(*2*, *34*). Equipped with two coil-coil domains, FRI is proposed to act as a scaffold protein, facilitating interactions with various *FLC* transcriptional regulators and chromatin remodelers. Nevertheless, FRI itself does not directly interact with the *FLC* gene locus. Instead, SUF4 serves as a mediator of this interaction by physically binding both *FLC* and FRI, along with many other members associated with the FRI complex (*3*, *37*). Thus, based on these previous findings and our observations that SUF4 forms relatively stable thermally-driven condensates compared to FRI, we propose a revised model in which SUF4 also plays an essential role as part of the regulatory scaffold at the *FLC* locus (Fig. 4). Through both condensation and its ability to recognize the *FLC* promoter region, SUF4 has the potential to recruit and concentrate transcriptional activators (e.g. previously reported SUF4 interactors FLX and TAF14), and chromatin remodelers (e.g. ELF7, SWC6, and RVB1) at the *FLC* promoter. Meanwhile, we hypothesize that FRI transiently interacts with SUF4, contributing to the establishment of transcriptional regulation of *FLC* in newly formed tissues such as lateral roots. Newly developed and emerging molecular images and technologies, such as those that enable the visualization and quantitation of molecular events at a single genetic locus (e.g., endogenous fluorescent tagging of gene loci via dCAS9/CRISPR), will aid in further investigating the functional dynamics that govern these interactions at the *FLC* gene locus.

The coacervation of prion-like proteins (PrLPs), such as FLL2 and FCA, has recently emerged as a potential regulatory mechanism in flowering time (*12*). However, it remains uncertain whether PrLP coacervation is thermally-driven, or even contributes to the post-transcriptional regulation of *FLC*. In this study, we demonstrate that a distinct proline-rich IDP undergoes LCST condensation behavior, which likely serves as a means to modulate flowering. This behavior aligns with the LCST observations of synthetic elastin-like proteins and Pab1(*24*, *38–41*) which also possess a high proline content and repetitive hydrophobic features. While plants carry numerous proline-rich proteins and hybrid proline-rich proteins that are involved with abiotic- and biotic-associated pathways, the thermo-induced coacervation behavior of these proteins remains underexplored. By unraveling the role of proline-rich IDPs in phase separation and its relevance to flowering time regulation, our study extends our understanding of proline-rich IDPs in biological processes and sheds light on their potential participation in eukaryotic thermo-responses through phase separation phenomena. Moreover, our findings provide a strong basis for exploring the role of phase separation and environmental sensing, providing a valuable foundation and new insights into how we may be able to engineer plants and other organisms with tailored environmental responses.

Despite IDPs being often poorly conserved (*42*, *43*), SUF4 shares substantial homology with the animal protein BuGZ. In these organisms, BuGZ plays essential roles in both mitotic and transcriptional regulation by interacting with various cellular machineries, including the spindle assembly checkpoint protein (SAC) Bub3, the spliceosome, and epigenetic factors (*13*, *14*, *44*). While SUF4's primary function in plants revolves around regulating flowering time, recent research has unveiled its potential involvement in analogous mitotic and transcriptional regulatory processes (*45–47*).These newfound roles raise a series of questions, including whether SUF4's phase separation has evolved distinct functionality specific to plant flowering or if it serves as a universal mechanism within eukaryotic systems. Interestingly, animal BuGZ has been observed to undergo phase separation *in vitro*, and its role in phase separation is hypothesized to

contribute to mitotic spindle formation. Therefore, studying SUF4 may not only advance our comprehension of how environmentally-induced phase separation impacts plant development and physiology but also hold significant promise in deepening our understanding of the broader evolutionary significance and functional implications associated with such environmentally-induced phase separation.

The strong correlation observed between SUF4's thermally-regulated condensation and flowering time highlights SUF4's significance as a genetically-tractable system for investigating the functional relevance of phase separation in plants, particularly in the context of their response to changing environmental conditions. Additionally, it offers invaluable insights into the fundamental organization and regulation of dynamic cellular processes that govern eukaryotic organisms.

MATERIALS AND METHODS:

Plant Material, accessions, and growth conditions

All plants used in this study were grown under controlled conditions in growth rooms with a light intensity of approximately 180 µmol m−2 s−1 at a temperature of 21°C. Plants were either exposed to long day conditions (16 hours of light followed by 8 hours of darkness) or short day conditions (8 hours of light followed by 16 hours of darkness).

Col (FRI-SF2) (*48*) was used as the wild-type accession for all genotypes analyzed in this study. These lines are characterized as winter annuals and exhibit a delayed flowering phenotype.

suf4 (FRI-SF2) plants (*29*) were used as the mutant accession for this study. These plants carry an ~6kb deletion that spans the N-terminus of SUF4 (deleted region: exons 1,2,3 and part of intron 3), resulting in a null mutation that causes an early flowering phenotype.

Transgenic lines generated in this study
pSUF4::mEGFP-SUF4 in *suf4 (FRI-SF2)*
pSUF4::mEGFP-5SSUF4 in *suf4 (FRI-SF2)*
pSUF4::mEGFP-12SUF4 in *suf4 (FRI-SF2)*
pFRI::FRI-mScarletI; pSUF4::mEGFP-SUF4 in *suf4 (FRI-SF2)*
pFRI::FRI-mScarletI; pSUF4::mEGFP-5SSUF4 in *suf4 (FRI-SF2)*
pFRI::FRI-mScarletI; pSUF4::mEGFP-12SSUF4 in *suf4 (FRI-SF2)*

Transgenic lines generated in this study
pELF7::mTFP-ELF7; pFRI::FRI-mScarletI; pSUF4::mEGFP-SUF4 in *suf4 (FRI-SF2)*

Flowering time quantification
To assess flowering time in SUF4 variants, seeds of each genotype were individually sown in Pro Mix BX soil and stratified at 4°C for two days. Then, planted pots were transferred to either short day or long day chambers. The total number of true rosette leaves was recorded until plants bolted. To minimize position effects, all genotypes were spatially mixed within their respective short- or long day growth chambers.

Cloning schemes:

pHM11 (rescue SUF4):
To create pHM11 (pSUF4::6HIS-mEGFP-SUF4), a 2,981 fragment containing the genomic SUF4 sequence was amplified using oHM3 (TTA GGA TCC GGT GGA GGC GGT TCA GGC GGA GGT GGC TCT GGC GGT GGC GGA TCG ATG GGT AAG AAG AAG AAG AGA), a forward primer with an added BamHI site and a 3XGGGS linker, and oHM4 (GGC CTC GAG CTA AAA CGC CAT CCG CCC AGC AA), a reverse primer with a 3' XhoI site. This fragment was then cloned into pGEM-T easy to generate pHM1 (genSUF4). Additionally, the mEGFP gene was amplified from addgene's commercially available mEGFP plasmid (#18696) using oHM1 (ATA AGA TCT AGT GAG CAA GGG CGA GGA G), a primer with a BglII 5' site, and oHM2 (ATG GAT CCC TTG TAC AGC TCG TCC ATG CC), a primer with a 3' BamHI site. The resulting fragment was cloned into pGEM-T easy to create pHM2 (mEGFP). Subsequently, pHM2 was digested with BglII and BamHI, and then inserted into the pET-30a(+) vector, resulting in pHM3 (6HIS-mEGFP). Plasmids pHM1 and pHM3 were then cleaved with BamHI and XhoI and ligated, yielding pHM4 (6HIS-mEGFP-SUF4). A 1059 bp fragment upstream of the SUF4 coding region was PCR amplified using oHM28 (ATC TTT AAC TTT TTT GTT GTT GCA) and oHM24 (GAT GGC GCG CCC ACT AAA TCT TTC TCC TA), a primer with an ASCI site, and inserted into the pGEM-T easy vector, generating pHM5 (proSUF4). Additionally, a 332 bp region downstream of the SUF4 coding region was PCR amplified using oHM25 (GAT GGC GCG CCC TCG AGA ATT TGG CAC CAA ACC AA), a primer with both ASCI XHOI restriction sites, and oHM17 (gaacaacatggtgcaaacatt), and cloned into pGEM-T easy to produce pHM6 (termSUF4). Subsequently, pHM5 was digested with SacII and AscI, and the resulting fragment was cloned into pHM6 to create pHM7 (proSUF4::AscI-XhoI-3'UTR). pHM4 (6HIS-mEGFP-SUF4) was reverse amplified to add a kozak consensus sequence using primers ohm45 (TTCACCAAAATGCACCATCATCATCATCAt) and oHM46 (GGcgcgCCCACTAAATCTTTCTCC), and then digested with AscI and XhoI for cloning into pHM7, resulting in pHM10 (proSUF4::6HIS-mEGFP-SUF4-3'UTR). For downstream biochemical assays requiring removal of mEGFP, an enterokinase sequence was introduced before the SUF4 coding region using primers oHM35 (CGATCCGCCACCGCCAGAGCC) and oHM36 (gacgacgacgacaagATGGGTAAGAAGAAGAAGAGA), generating pHM10_entero

(proSUF4::6HIS-mEGFP-entero-SUF4-3'UTR). Subsequently, pHM10_entero was cloned into pBIN30 via the NotI restriction site to make pHM11 (proSUF4::6HIS-mEGFP-entero-SUF4-3'UTR) .

pHM32 (30I SUF4):
To create pHM32, the last 1969 bp of SUF4's disordered region was synthesized (GenScript, USA) with base pair substitutions that replaced all 30 alanine residues with isoleucine residues. Gibson assembly was used to fuse this fragment with the remaining 1012 genomic sequence of SUF4 to reassemble the complete gene. Once the 30I SUF4 fragment was assembled, pHM10_entero and the 30I fragment were cut with BamHI and XhoI and ligated together to make pHM31 (pSUF4::mEGFP-30ISUF4). Then, pHM31 was cut with Not1 and cloned into the binary vector pBIN30 (Basta resistant) to make pHM32 (pSUF4::mEGFP-30ISUF4).

pHM14 (12S SUF4):
To create pHM14, the last 1969 bp of SUF4's disordered region was synthesized (GenScript, USA) with base pair substitutions that replaced 12 of the 14 phenylalanine and lysine residues with serines. Gibson assembly was used to fuse this fragment with the remaining 1012 genomic sequence of SUF4 to reassemble the complete gene. Once the 12S SUF4 fragment was assembled, pHm10_entero and the 12S fragment were cut with BamHI and XhoI and ligated together to make pHM12 (pSUF4::mEGFP-12SSUF4). Then, pHM12 was cut with Not1 and cloned into the binary vector pBIN30 (Basta resistant) to make pHM14 (pSUF4::mEGFP-12SSUF4).

pHM5S (5S SUF4):
To create pHM5S, the last 1969 bp of SUF4's disordered region was synthesized (GenScript, USA) with base pair substitutions that replaced the last 5 phenylalanine and lysine residues with serines. Gibson assembly was used to fuse the remaining 1012 genomic sequence of SUF4 to reassemble the complete gene. Once the 5S SUF4 fragment was assembled, pHm10_entero and the 5S fragment were cut with BamHI and XhoI, and ligated together to make pHM13 (pSUF4::mEGFP-5SSUF4). Then, pHM13 was cut with Not1 and cloned into the binary vector pBIN30 (Basta resistant) to make the final vector pHM5S (pSUF4::mEGFP-5SSUF4).

pFRI::FRI-mScarletI:
pFRI::FRI-mScarletI was custom-synthesized by GenScript and consists of the following elements: The FRI 1243 bp upstream promoter region with an added Kozak consensus sequence (CACCAAA), directly followed by the 1351 bp FRI (SF2) genomic region, 3XGGGS linker (GGT GGA GGC GGT TCA GGC GGA GGT GGC TCT GGC GGT GGC GGA TCG), mScarletI sequence derived from Addgene 98839, and FRI's putative 169 bp 3'UTR. Both promoter and 3'UTR sequences were obtained from TAIR Sequence Viewer, whereas the genomic sequence was provided by Sang Yeol Kim. The aggregated synthesized DNA was flanked with NotI cut sites and subsequently inserted into the pBIN40 (Hyg resistant) binary vector through NotI digestion and ligation.

pELF7::mTFP-ELF7:

pELF7::mTFP-ELF7 was custom synthesized by GenScript, USA and comprises the following components: The ELF7 405 bp upstream promoter region with an added Kozak consensus sequence (CACCAAA), directly followed by the mTFP sequence (Addgene 55503), 3XGGGS linker (GGT GGA GGC GGT TCA GGC GGA GGT GGC TCT GGC GGT GGC GGA TCG), the 3228 bp ELF7 genomic region (TAIR), and the ELF7 putative 1791 bp 3' UTR. All promoter, genomic, and 3'UTR sequences were obtained from TAIR Sequence Viewer. The synthesized DNA was flanked by NotI sites, which were used for subsequent insertion into the pBIN40 (Hyg resistant) binary vector.

Confocal microscopy and analysis

All confocal imaging was performed either using lightning deconvolution mode on a Leica SP8 point scanning confocal microscope or with a spinning disk confocal microscope. The Leica SP8 was equipped with a leica hcx pl apo 63x 1.30 glycerol objective, whereas the spinning disk confocal head (QLC100: Yokogawa) was mounted on a DMA6000B microscope (Leica) using a 100x Plan-Apo 1.4 NA oil-immersion objective. Each sample was either excited using a GFP 488nm (Coherent cube laser), mScarletI at 561nm (Coherent sapphire laser), or mTFP at 442nm (Coherent cube laser).

Fluorescence Recovery After Photobleaching (FRAP)

FRAP was performed using a spinning disk (CSU-X, Yokogawa Corp.) confocal microscope equipped with a Vector galvometer beam steering unit (Intelligent Imaging Innovations) attached to the right camera port of a fully automated Leica DMI6000 microscope to direct focused laser energy to the image plane. The camera port was switched via software control (SlideBook, Intelligent Imaging Innovations) to alternate between imaging and FRAP light paths. mEGFP-SUF4 was imaged using 3.5 mW of light energy (as measured at the end of the laser fiber entering the confocal head) from a solid state 488nm laser (Coherent Technologies). Emission light was collected using a 488nm dichroic mirror and 500-550nm emission filter (Semrock). Single-plane Images were collected every 200ms using a Leica 100x Plan-Apochromat 100x 1.40 NA oil immersion objective and FRAP was performed within a 1.094 micron^2 region of interest centered on each assessed condensate spot using 5mW of light energy as measured at the end of the fiber entering the Vector unit. The focal spot was moved by galvometers to bleach a grid of spots separated by 20 nm within the FRAP region. Seven frames were collected before bleaching and 143 frames were collected after bleaching (1.75 seconds to conduct bleaching, 0.2 second delay to first post-bleach acquisition). Once all images were acquired, they were aligned in ImageJ (*49*) using the MultiStackReg plugin (*45*). The Trackmate plugin (*50*) was used to segment mEGFP-SUF4 spots for measurement of both the mean fluorescent intensity and mobility of condensates over time (DoG detector, estimated object diameter 0.6µm, sub-pixel localization, simple LAP tracker: Linking max distance 1µm, Gap-closing distance 1µm, and Gap-closing max frame gap 1). Afterwards, easyFRAP(*51*) (https://easyfrap.vmnet.upatras.gr/) was used to calculate double normalized FRAP values among the different variants, with each curve undergoing a double exponential curve fit (Normalization method: Double, Exponential Equation: Double, Data collected: T-Half, Mobile Fraction, R-Squared).

Live-cell imaging during temperature change

Live-cell imaging was performed on roots of 6-7 day old seedlings using a Leica SP8 point scanning confocal microscope equipped with HyD detectors, a white light supercontinuum laser, and AOBS (Acousto-Optical Beam Splitter) control of shuttering, excitation and emission bands. All images were acquired with a Leica glycerin immersion 60x 1.3 N.A. Plan Apochromat Leica objective. Seedlings were placed in a 4C growth chamber for 24 hours. Then, they were mounted in ice water and moved onto the microscope stage, where they underwent continuous imaging for 10 minutes. As a control, room temperature seedlings were mounted in room temperature water and continuously imaged using the same amount of time.

Colocalization analysis

Co-localization of mEGFP-SUF4 condensates with FRI-mScarletI, U2B", and/or mTFP-ELF7 were performed in multichannel 3D datasets where image planes were acquired at 0.3µm intervals. The Spots function and Matlab plugin for colocalization analysis in Imaris (RRID:SCR_007370, URL:http://www.bitplane.com/imaris/imaris) were used to segment condensate signal and assess co-localization. Spot diameters of 0.5µm were used to detect and determine the locations of mEGFP-SUF4, whereas FRI and U2B" condensates were detected with a spot diameter of 0.7µm. These diameters values were determined by assessing the diameter that worked best for segmentation of condensate signal using the Imaris Spots function and were largely indicative of the typical condensate diameters. Spots were considered co-localized if the centroids of the spots (determined at a sub-pixel scale), were closer than the radius of the smaller Spot size used to detect and segment mEGFP-SUF4 signal (0.25 µm).

Puncta quantification

To quantify SUF4 nuclear condensates, we auto-cropped individual nuclei from 3D stacks using the NucleusJ2.0 auto crop function in Fiji. Subsequently, the cropped images were imported into LabView, where a custom signal algorithm was applied to normalize the signal loss due to light scattering and spherical aberration from the top to the bottom of the z-stacks. To create the dataset used for normalization, we isolated the diffuse EGFP-SUF4 signal within the nucleoplasm away from the brighter SUF4 puncta via a set of binary masks, one mask for total SUF4 signal above background and second mask for the puncta. The threshold for the total mask was set by eye, and that for the puncta was created to include only pixels falling between 0.02% and 20% below the maximum pixel value in the section. For each section, the puncta signal was then subtracted from the total signal to obtain the nucleoplasm signal, and the mean nucleoplasm value per pixel calculated. The nucleoplasm signal was roughly linear to the focal depth once the focal plane was within the nuclear volume, enabling us to model signal loss with a linear fit to the mean intensity in these focal sections. The pixels in planes conjugate the nuclear volume were normalized to the inverse of the fit line. The code for TIFF file reading was shared online by Brian Hoover(forums.ni.com), the code for TIFF multipage saving was shared online by Nico (forums.ni.com)and used with modifications.

Statistical analysis

For the analysis of flowering time and condensate numbers, a nonparametric Mann-Whitney U test was used to test for statistically significant differences among sets of measurements made in different genotypes. For qPCR, FRAP and motility results, a Student's two-tailed T-test for independent means was used. To assess the significance of the co-localization rate between FRI-mScarletI and mEGFP-SUF4 condensates, we chose to compare the observed frequency of co-localization with mEGFP-SUF4 to another nuclear condensate, U2B"-mRFP, which forms 1-2 puncta per nucleus of similar sizes to those observed for FRI-mScarletI, and for which there was no prior expectation of possible co-localization. The reason for this approach, rather than a method involving calculating the likelihood of observed coincidence of a known number of objects in a measured volume, a two-sample (binomial) test of proportions was used to analyze the results.

QPCR

qPCR was employed to assess the transcript levels of both *SUF4* and *FLC*. To achieve this, total RNA was extracted from six-day-old seedlings (approximately 20 seedlings per genotype) using the NucleoSpin RNA plant kit (Macherey-Nagel CO.). Subsequently, 1 microgram of total RNA was reverse transcribed using the QuantiTect Reverse Transcription kit (Qiagen). Real-time RT-PCR was performed on 1:10 diluted cDNA using the SensiFAST SYBR No-ROX Kit (Bioline). Three biological and technical replicates were analyzed per genotype, and ROC1 (AT4G38740) was used as a reference gene to normalize gene expression. The reactions were carried out with an initial denaturation step at 95°C for 2 min, followed by 45 cycles of 95°C for 5 s, 60°C for 10 s, and a final step at 72°C for 5 s.

Primer name	Sequence	5' or 3'	Amplified gene
FLC Forward	TCTCCTCCGGCGATAACCT	5'	*FLC*
FLC Reverse	GCATGCTGTTTCCCATATCGAT	3'	*FLC*
SUF4 Forward	AGGAATTCCACCCCATGTCTTGAC	5'	SUF4
SUF4 Reverse	CTGAGATTCGTCTGTCTATCGC	3'	SUF4
Cyclo Forward	CGATAAGACTCCCAGGACTGCCGA	5'	ROC1
Cyclo Reverse	TCGGCTTTCCAGATGATGATCCAACC	3'	ROC1

Expression of His-mVenus-SUF4 in Sf9 cells

Cloning and expression of His-mVenus-SUF4 was based on Bac-to-Bac Baculovirus Expression system (ThermoFisher). The control pFastBac-mVenus and pFastBac-mVenus-SUF4 isoform 1 plasmids were obtained from Dr. Alex Chin (*15*). In these vectors, mVenus was cloned solely or with an open reading frame of SUF4 isoform 1 (NP_564369.1; 367 amino acid) in the modified pFastBac vector (ThermoFisher). Site-directed mutagenesis was carried out to create the 5S and 12S mutants using PrimeSTAR Max DNA polymerase (Takara-bio). All plasmids were sequenced and verified prior to the transformation of DH10Bac. Bacmid preparation, transfection and infection of Sf9 cells were performed according to the manufacturer's instruction. The large scale protein expression was carried out by infecting and culturing the Sf9 cells with P3 viruses for 2 days. Cells were centrifuged and either used immediately for protein purification or frozen and stored at -80°C until use. Purification of His-mVenus-SUF4 fusion protein from Sf9 cells. His-mVenus-SUF4 proteins were purified with IMAC followed by gel filtration as published previously with some modifications. All procedures were performed at 4°C. Proteins were extracted by sonicating the cells in lysis buffer [50 mM Tris, 500 mM NaCl, 20 mM imidazole, 5 mM TCEP (SIGMA, C4706), 5% glycerol, protease inhibitor cocktail (SIGMA, S8830) pH 7.44] supplemented with benzonase nuclease (SIGMA, E1014). The lysate was cleared by centrifugation at 20,000 x g, for 20 min at 4°C, filtered with 0.45 µm PVDF membrane filter (Millipore, SLHV033RS) and loaded onto Ni-NTA columns (QIAGEN, 30230). After washing with the lysis buffer, proteins were eluted with 500 mM imidazole (lysis buffer supplemented with 480 mM imidazole). The eluate was concentrated using a centrifugal filter device, Amicon Ultra-15 (Millipore, UFC901024) and loaded to a gel filtration column Superdex 200 Increase 10/300 GL operated with AKTA Pure 25L (GE Healthcare). Gel filtration was performed in the Size Exclusion Chromatography (SEC) buffer (20 mM Hepes, 225 mM NaCl, 1 mM TCEP pH 7.4) with a constant flow rate of 0.4 ml/min. Typically, His-mVenus-SUF4 and His-mVenus proteins were eluted at 11.0 and 15.5-ml after the protein loading, respectively. Obtained fractions were analyzed with SDS-PAGE, combined and concentrated. Protein concentration was determined with Bradford protein assay kit (Thermo, 23200) using BSA as a standard.

Turbidity assay

His-mVenus or His-mVenus-SUF4 proteins were thawed and ultracentrifuged to remove denatured proteins. After protein concentration was determined, the protein sample was diluted to 50, 25, 12.5, 6.25 and 3.13 µM in SEC buffer. Each sample was mixed well with equal volume of turbidity assay buffer (20 mM Hepes, 75 mM NaCl, pH 7.4) to make a 250 µl reaction mix and transferred into a quartz cuvette (Starna Cells, 28F-Q-10). Temperature-dependent phase transition was detected by measuring the optical disturbance at 800 nm by increasing the temperature from 4 to 60°C (with a ramping rate of 0.5°C/min) using a spectrophotometer Cary 300UV-VIS (Agilent Technologies). Nitrogen gas purging was used to prevent the moisture from condensing on the cuvette surface.

Droplet formation assay

Five microliter of 50 μM proteins prepared as described above were mixed with 5 μl of turbidity assay buffer on ice and incubated for 5 min at 37°C. Each 3 μl of protein reaction mix was loaded into a flow-chamber and immediately observed with a confocal microscope SP5 (Leica) equipped with a 60x oil objective (NA 1.42). Imaging was performed with both DIC and fluorescence (excitation at 514 nm, emission 530 nm).

FIGURES:

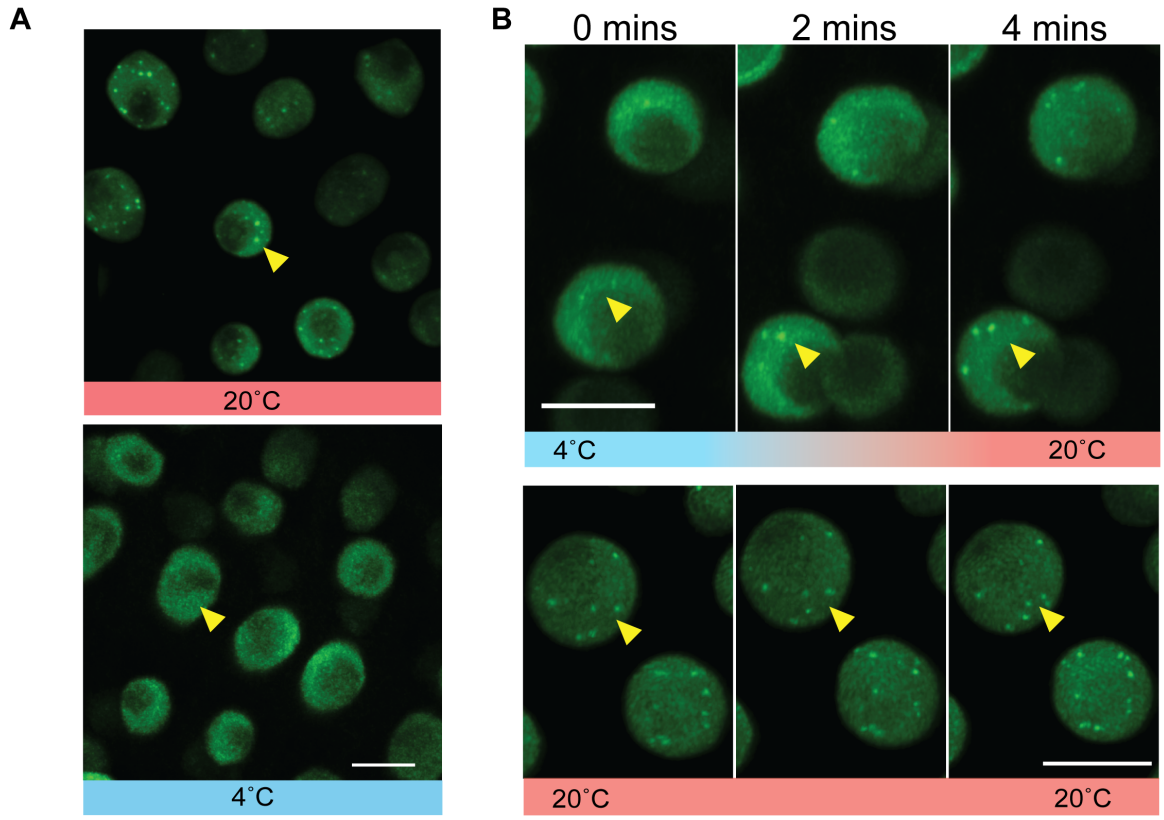
A
20˚C
4˚C
B
0 mins
2 mins
4 mins
4˚C
20˚C
20˚C
20˚C

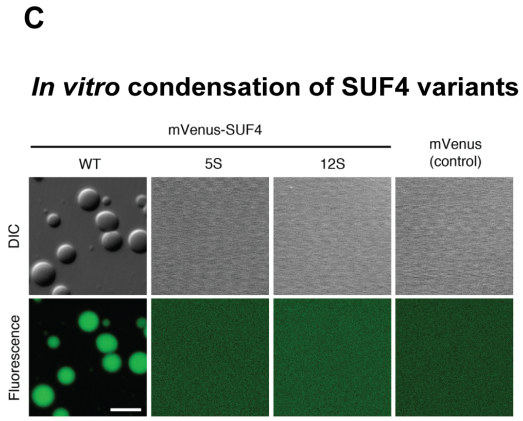
C
In vitro condensation of SUF4 variants
mVenus-SUF4
WT
5S
12S
mVenus (control)
DIC
Fluorescence

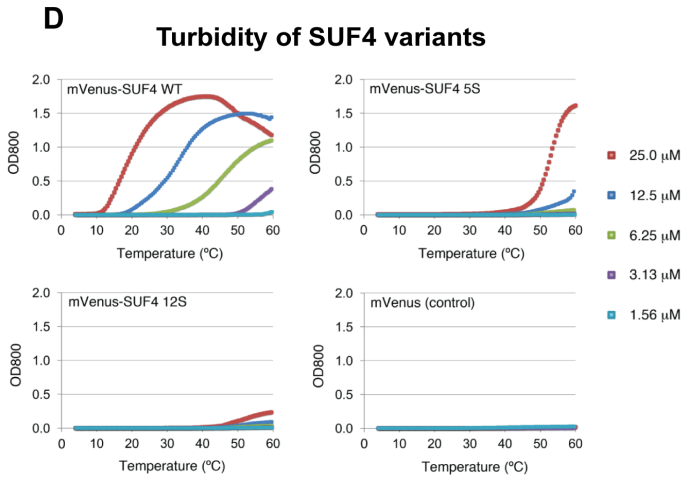
D
Turbidity of SUF4 variants
mVenus-SUF4 WT
mVenus-SUF4 5S
mVenus-SUF4 12S
mVenus (control)
OD800
Temperature (ºC)
25.0 µM
12.5 µM
6.25 µM
3.13 µM
1.56 µM

Figure 1. SUF4 forms nuclear condensates that are sensitive to temperature *in planta* and *in vitro*. A) SUF4 is diffuse within the nucleoplasm and forms nuclear condensates at room temperature. However, at 4°C, it remains only diffuse in the nucleoplasm. **B)** SUF4 rapidly forms condensates as temperatures increase. Scale bar= 10µm, yellow arrowheads point to nuclei either with the presence or absence of nuclear condensates. **C)** DIC and confocal images of purified SUF4 variants. Only rescue SUF4 forms condensates at 37°C. Scalebar for *in vitro* SUF4 = 5µm, **D)** Turbidity assay demonstrating the temperature sensitivity of purified SUF4 variants. The thermal setpoints shift depending on the severity of amino acid substitutions and the concentration used.

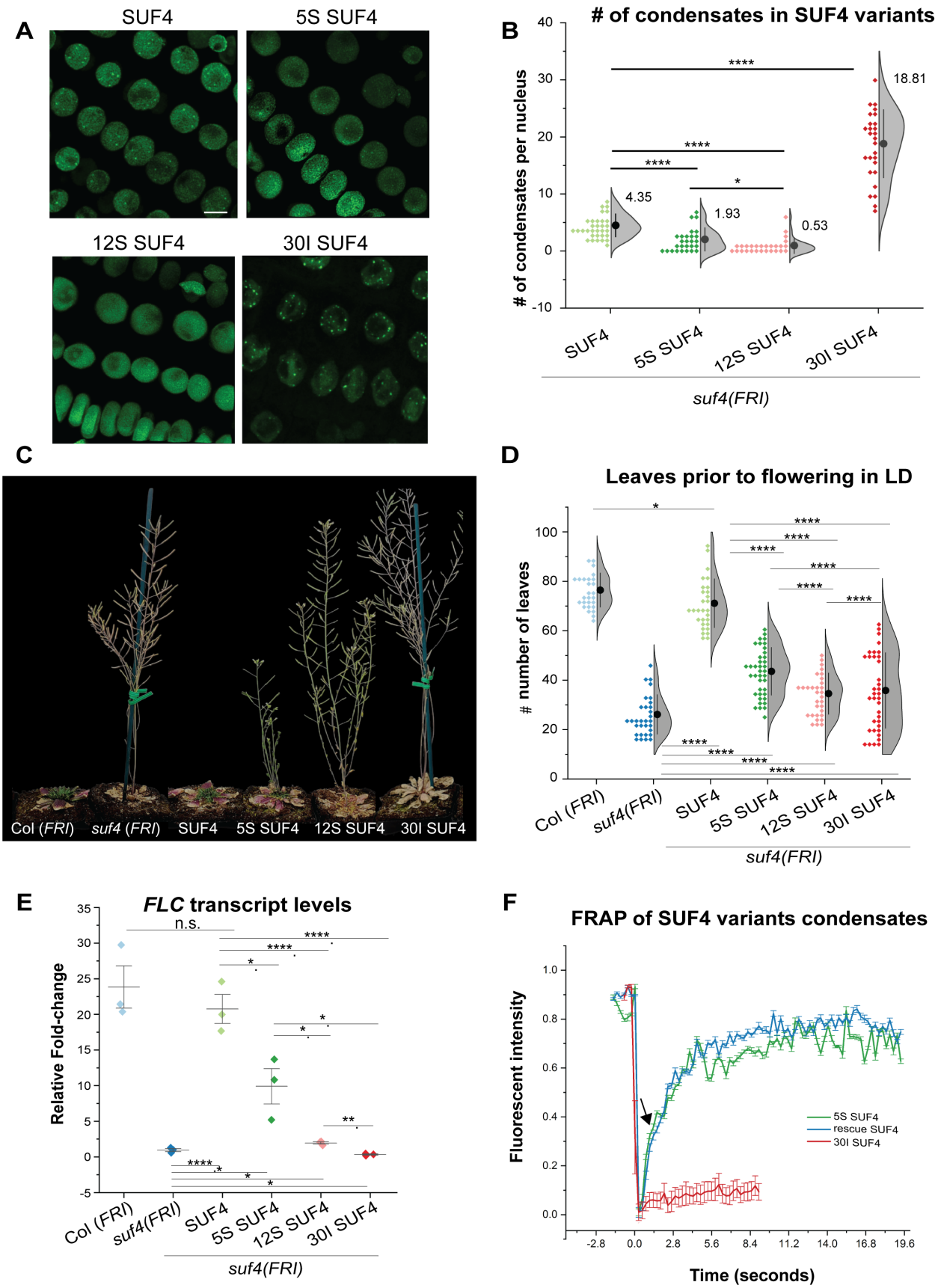
A
SUF4
5S SUF4
12S SUF4
30I SUF4
B
# of condensates in SUF4 variants
# of condensates per nucleus
4.35
1.93
0.53
18.81
SUF4
5S SUF4
12S SUF4
30I SUF4
suf4(FRI)
C
Col (FRI)
suf4 (FRI)
SUF4
5S SUF4
12S SUF4
30I SUF4
D
Leaves prior to flowering in LD
number of leaves
Col (FRI)
suf4(FRI)
SUF4
5S SUF4
12S SUF4
30I SUF4
suf4(FRI)
E
FLC transcript levels
Relative Fold-change
n.s.
Col (FRI)
suf4(FRI)
SUF4
5S SUF4
12S SUF4
30I SUF4
suf4(FRI)
F
FRAP of SUF4 variants condensates
Fluorescent intensity
5S SUF4
rescue SUF4
30I SUF4
Time (seconds)

Figure 2. Tuning SUF4 condensate behavior corresponds to changes in flowering time outcomes. A) Confocal images of distinct SUF4 variants, illustrating varying condensation patterns. Rescue mEGFP-SUF4 forms an average of 4-5 nuclear condensates; 5S SUF4 forms 2-3 nuclear condensates on average; 12S SUF4 shows 0-1 condensates on average; and 30I SUF4 forms an average of 16-17 nuclear condensates. **B)** Quantification of panel A). Mean condensate values are indicated next to each plot. Statistical analysis was performed with a Mann Whitney U test. **C)** Image of plants expressing various mEGFP-SUF4 variants alongside wildtype (Col(FRI)) plants. Left to right: WT (Col(FRI)) with delayed flowering, suf4(FRI) mutant with early flowering, rescue mEGFP-SUF4 (functional copy of SUF4) rescuing the flowering time, 5S SUF4 (5 Y and F substitutions for S) with weak early flowering, 12S SUF4 (12 F and Y substitutions for S) with moderate early flowering, and 30I SUF4 (30 A to I substitutions) with early flowering. **D)** Quantification of A) Statistical analysis performed using a Mann-Whitney U test. **E)** Relative abundance of *FLC* transcripts in different SUF4 variants. Rescue SUF4 shows FLC transcript levels similar to WT, while various substitutions lead to graded reductions. Statistical analysis conducted using a two-tailed Studen't t-test for independent means. Error bars represent the standard deviation. **F)** Fluorescence Recovery After Photobleaching (FRAP) Results: FRAP analysis of SUF4 variants reveals different recovery rates. Notably, 5S SUF4 exhibits the fastest recovery rate ($t_{1/2}$=0.85 seconds), followed by rescue SUF4 ($t_{1/2}$=1.27 seconds, denoted by arrow), while 30I SUF4 does not recover within the experiment's duration. FRAP distributions between rescue and 5S SUF4 were assessed for significance using a two-tailed Student's t-test (p-value=0.007). Asterisks denote specific p-values * <0.01, ** <0.001, ***<0.001, and ****<0.0001. Error bars= standard deviation.

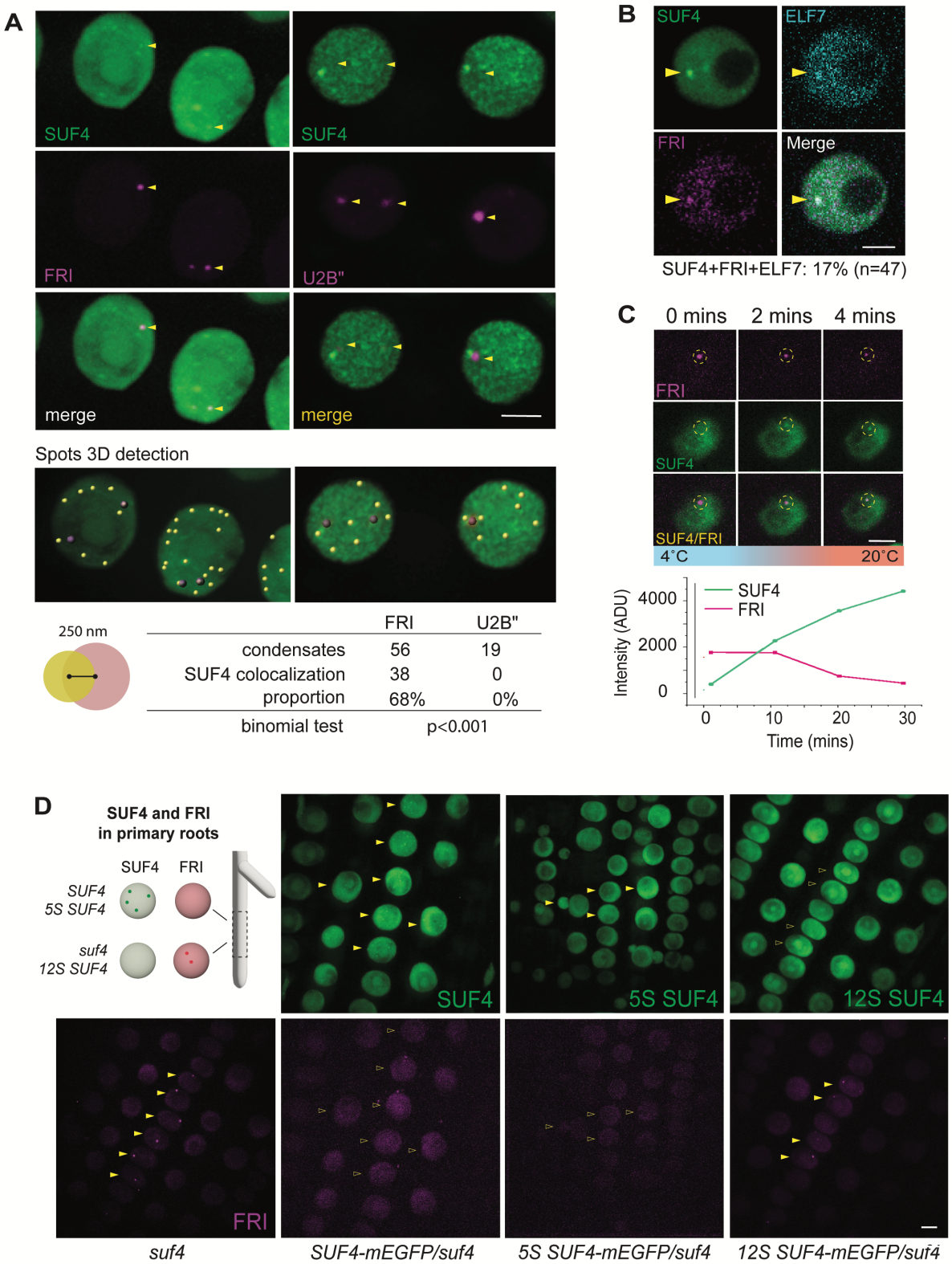

	FRI	U2B"
condensates	56	19
SUF4 colocalization	38	0
proportion	68%	0%
binomial test	p<0.001	

Figure 3. SUF4 co-localizes with members of the vernalization complex in newly derived meristematic tissues. A) Co-Localization of SUF4 and FRI in Nuclear Condensates within developing Lateral Roots at room temperatures. This co-localization appears to be selective, as SUF4 and U2B", a protein found in nuclear splicing speckles, remains separate from SUF4. Binomial tests of proportions used to test for statistical significance. **B)** ELF7, a chromatin remodeler that functions known to interact with SUF4 and FRI to transcriptionally activate *FLC* also co-localizes within SUF4-FRI condensates. **C)** Cold-induced FRI condensates do not co-localize with SUF4. However, these condensates can exchange positions with SUF4 nuclear condensates upon warming. First 20 minutes of imaging data are shown (three time points). Graph is of single image series but with one additional time point (30 minutes, four time points). Dotted circle is not the ROI used for quantification but used to mark diminishing and appearing condensates. **D)** SUF4 condensates spatially limit the formation of FRI condensates in the primary root. In SUF4 variant lines lacking condensates (12S and *suf4* mutants), FRI-mScarletI condensates begin to emerge. Scale bars: 5µm

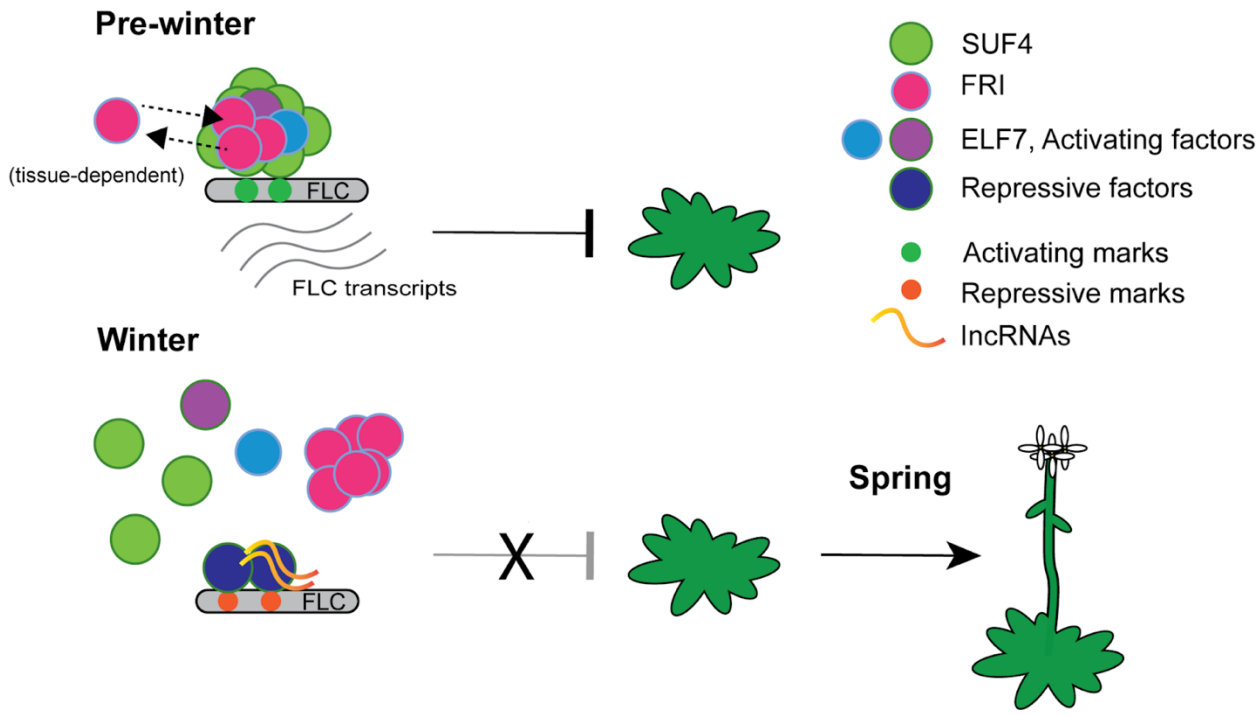

Figure 4: Proposed Model for Flowering-Time Regulation. This figure illustrates a proposed model for the regulation of flowering time mediated by SUF4 biomolecular condensates. SUF4 (green) biomolecular condensates function to concentrate and/or recruit members of the vernalization complex, including FRI (in red), ELF7 (in blue), and other associated factors (in purple) to the *FLC* gene locus. Certain members, such as FRI, exhibit transient localization within these condensates dependent on cell state. Condensate localization ultimately leads to the transcriptional activation of the *FLC* gene, resulting in the delay in flowering time. In response to cold temperatures, SUF4 condensates undergo disassembly. This disassembly facilitates the recruitment of a new group of chromatin remodelers and the involvement of lncRNAs, both of which work together to transcriptionally silence the *FLC* gene. Transcriptional silencing of FLC is a necessary step for plants to undergo the floral transition and flower in the subsequent spring season.

Supplemental Figures

A

suf4 (FRI) *Col (FRI)* *SUF4 / suf4(FRI)*

B

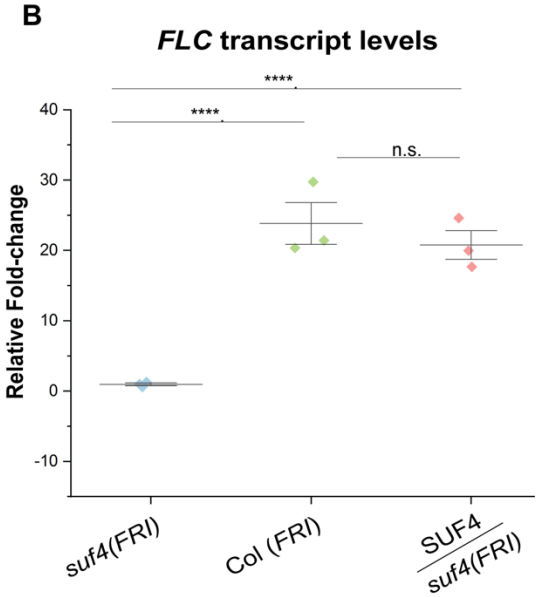

C

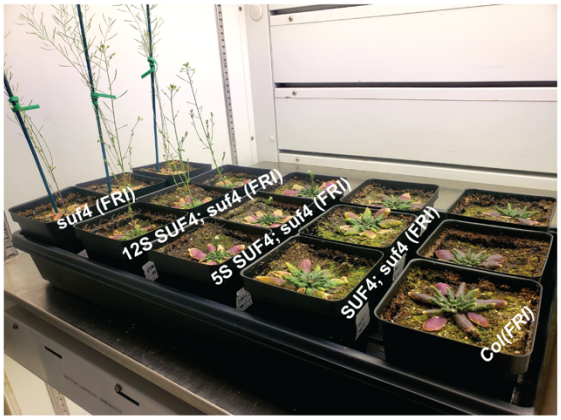

suf4 (FRI) *12S SUF4* *5S SUF4* *SUF4* / *suf4 (FRI)*

D

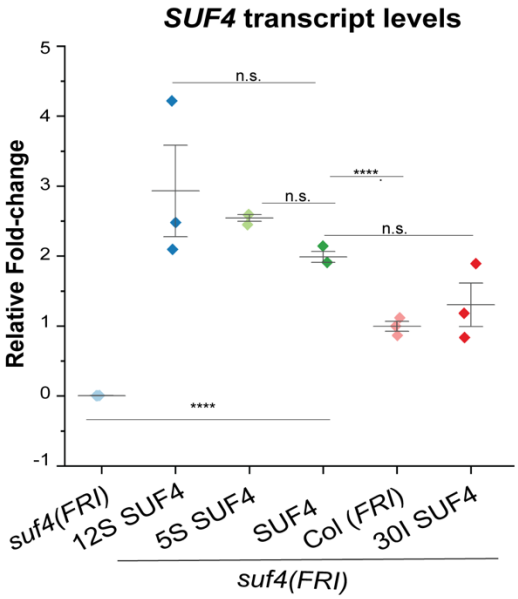

Supplemental Figure 1. Expression of pSUF4::mEGFP-SUF4 transgene rescues the *suf4* mutant phenotype **A)** Image of plants demonstrating the ability of the pSUF4::mEGFP-SUF4 transgene to rescue the *SUF4* flowering time phenotype. L-R: *suf4 (FRI)* mutant plants displaying an early flowering time phenotype, Col *(FRI)* plants displaying a WT delayed flowering time phenotype, SUF4/*suf4(FRI)* displaying a rescued WT delayed phenotype. **B)** Relative abundance of *FLC* transcripts in *suf4* mutant, Col *(FRI)*, and *SUF4 (FRI)* shown in A). Rescue SUF4 shows FLC transcript levels similar to WT. This data is reshown in Figure 2E. Statistical analysis conducted using a two-tailed t-test for independent means. Error bars represent the standard deviation. **C)** Two images of hydrophobic and hydrophilic variants of mEGFP-SUF4 in comparison mutant *suf4*, which flowers early. Top image L-R: *suf4 (FRI)* mutant with an early flowering time phenotype, 12S SUF4 (12 F and Y substitutions for S) with moderate early flowering, 5S SUF4 (5 Y and F substitutions for S) with weak early flowering, rescue mEGFP-SUF4 (functional copy of SUF4) rescuing the flowering time, and WT (Col (FRI)) with delayed flowering. Bottom image: same as top image but without WT (Col (FRI)). **D)** qPCR of *SUF4* in transgenic *SUF4* variant lines. Rescue *SUF4* is expressed approximately 2-folds over endogenous levels but expressed almost equally to other variants. Vertical lines equal the standard deviation. Asterisks denote the p-value of student's T-test * <0.01, ** <0.001, ***<0.001, and ****<0.0001.

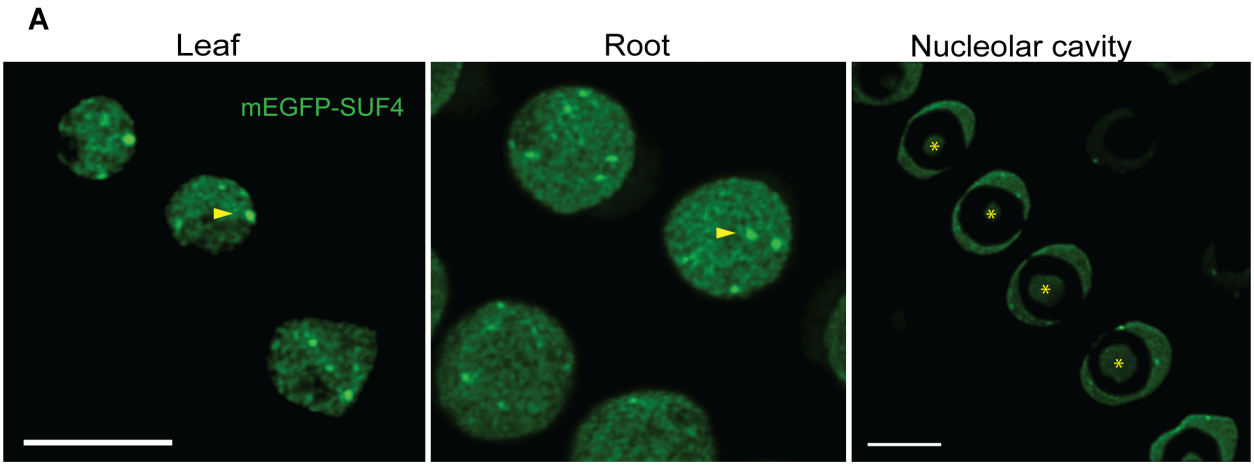

Supplemental Figure 2. At room temperatures, SUF4 forms biomolecular condensates in shoot cells, root cell, and localizes in the nucleolar cavity. Arrows point to nuclear condensates whereas stars mark the nucleolar cavity. Leaf and Root images are 3D rendered Z-stacks whereas the nucleolar cavity image is a slice from a 3D stack. Scalebar= 10 µm

```
Arabidopsis  1    MGKKKKRATEKVWCYYCDREFDDEKILVQHQKAKHFKCHVCHKKLSTASGMVIHVLQVHK   60
Mouse        1    MGRKKKK-QLKPWCWYCNRDFDDEKILIQHQKAKHFKCHICHKKLYTGPGLAIHCMQVHK   59
Xenopus      1    MGRKKKK-QLKPWCWYCNRDFDDEKILIQHQKAKHFKCHICHKKLYTGPGLAIHCMQVHK   59
                  **:***:    * **:**:*:*******:***********:***** *. *:.** :****

Arabidopsis  61   ENVTKVPNAKDGRDSTDIEIYGMQGIPPHVLTAHYGEEEDEPPAKVAKV-----------   109
Mouse        60   ETIDAVPNAIPGRTDIELEIYGMEGIPEKDMDERRRLLEQKTQESQKKK--QQDDSDEYD   117
Xenopus      60   ETIDAVPNAIPGRTDIELEIYGMEGIPEKDMEERRRILEQKTQVDGQKKKTNQDDSDYDD   119
                  *.:  ****  ** . ::*****:*** : :  :    *::   .  *

Arabidopsis  110  EIPSAPLGGVVPRP---YGMVYPPQQVP---------GAVPARPMYYPG-PPMRHPAP--   154
Mouse        118  DDESAASTSFQPQPVQPQQGYIPPMAQPGIPPVPGAPGMPPGIPPLMPGVPPLMPGMPPV   177
Xenopus      120  DDDTAPSTSFQ--QMQTQQAFMPTMGQPGIPGLPGAPGMPPGITSLMPAVPPLISGIPHV   177
                  :  :*   ..            *    *          *  *.     *. *    .

Arabidopsis  155  VWQMPPPR-PQQWYPQNPALSVPPAAHLGYRPQPLFPVQNMGMTPTPTSAPAIQPSPVTG   213
Mouse        178  MPGMPPGLHHQRKYTQSFC-----------GENIMMPMGGMM--PPGPGIPPLMPGMPPG   224
Xenopus      178  MAGMHP--------------------------HGMMSMGGMM-HPHRPGIPPMMAGLPPG   210
                  :  * *                              :: : .*   *   . * :  .   *

Arabidopsis  214  VTPPG----IPT-----------------------SSPAMPVPQPLPPVVNNSIPSQAPP   246
Mouse        225  MPPPVPRPGIPPMTQAQAVSAPGILNRPPAPTAAVPAPQPPVTKPLPPSAGQAQAAV---   281
Xenopus      211  VPPPGLRPGIPPVTQAQPALSQAVVSRLPVPSTSAPAL-QSVPKPLPPSAGQAQAHI---   266
                  : **     **                            :    * :**** ..::

Arabidopsis  247  FSAPLPVGGAQQPSHADALGSADAYPPNNSIPGGTNAH-------SYA----SGPNTSG-   294
Mouse        282  ---------------QGPVG--TDFKPLNSTPAATTTEPPKPTFPAYTQSTASTTSTTNS   324
Xenopus      267  ---------------SGPVG--TDFKPLNNIPAT-TAEHPKPTFPAYTQSTMSTTSTTNS   308
                                . :*    : * *. *.  .:.       :*:    *  .*:.

Arabidopsis  295  PSIGPPPVIANK--APSNQPNEVYLVWDDEAMSMEERRMSLPKYKVHDETSQMNSINAAI   352
Mouse        325  TAAKPAASITSKPATLTTTSATSKLIHPDEDISLEERRAQLPKYQRNLPRPGQTPIG---   381
Xenopus      309  TASKPSTSITSKPATLTTTSATSKLVHPDEDISLEEKRAQLPKYQRNLPRPGQAPISNMG   368
                   :  *   *:.*  : :.      *:  ** :*:**:* .****: :        *.

Arabidopsis  353  DRRISESRLAGRMAF-------------------------------------------   367
Mouse        382  NPPV--GPIGGMMPPQPGLPQ-QQAMRPPMPPHGQYGGHHQGMPGYLPGAMPPYGQGPPM   438
Xenopus      369  STAV--GPLGAMMAPRPGLPPQQHGMRHPLPPHGQYGAPLQGMAGYHPGTMPPFGQGPPM   426
                  .     . :.. *

Arabidopsis       --------------------------
Mouse        439  VPPYQGGPPRPPMGMRPPVMSQGGRY                                    462
Xenopus      427  VPPFQGGPPRPLMGIRPPVMSQGGRY                                    452
```

Supplemental Figure 3. Sequence alignment of *Arabidopsis* SUF4, mouse and Xenopus BuGZs. N-terminal domain that contains predicted NLS and zinc fingers (highlighted in cyan), is conserved well among three SUF4/BuGZ sequences whereas the central/C-terminal disordered domain of *Arabidopsis* SUF4 seems diverged from animal BuGZs. F and Y residues in the predicted disordered region are highlighted in black, blue, or purple. Other strong hydrophobic residues are highlighted in green. Among F and Y in the predicted disordered region of SUF4, the last 5 F and Y (highlighted in purple) were mutated to S in the 5S mutant and additional 7 F and Y at the central region (highlighted in blue) were mutated to the S in the 12S mutant.

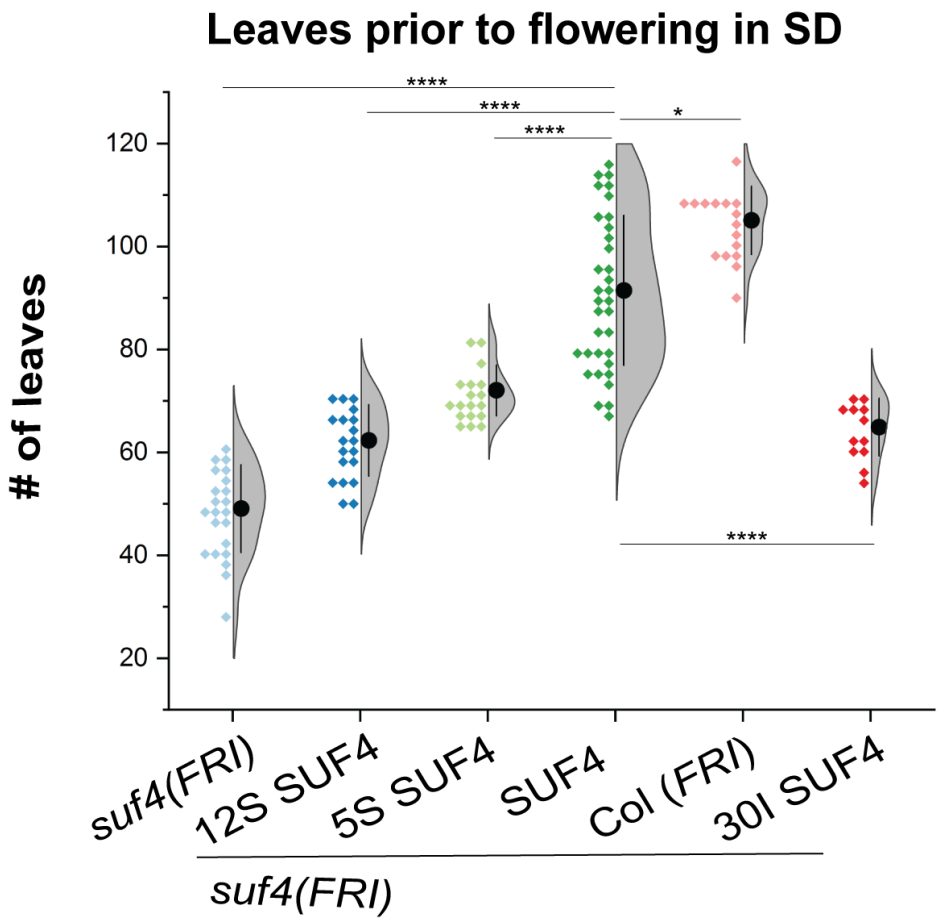

Supplemental Figure 4. Leaf counting assay of different variants in short day conditions. Similar flowering time results as in long day conditions from Figure 1B. Asterisks denote P-values from Mann-Whitney U test * <0.01, ** <0.001, ***<0.001, and ****<0.0001

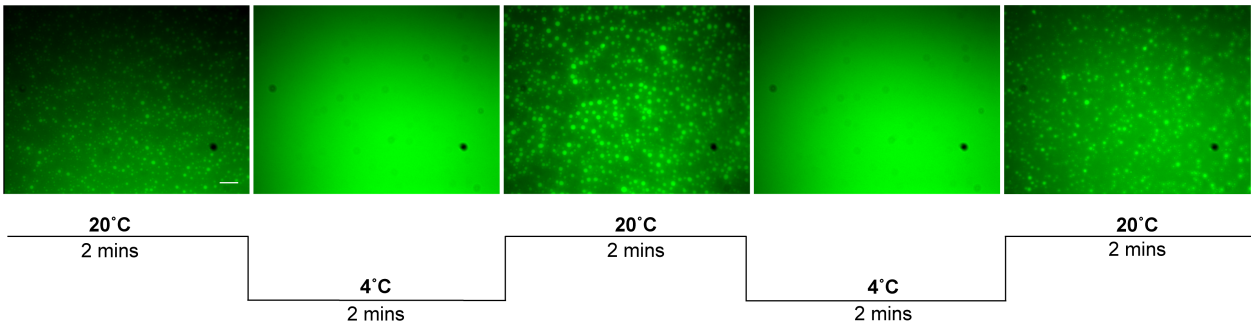

Supplemental Figure 5. Purified SUF4 forms round and reversible liquid-like condensates *in vitro*. SUF4 can undergo multiple rounds of temperature shifts without transitioning into a more stable gel or solid-like aggregate. Prior to temperature shifts, SUF4 is incubated at either 20˚C to 4˚C for 2 minutes. Upon temperature shifts every two minutes, SUF4 changes its phase state and maintains this behavior until the next shift. Scalebar = 45µm

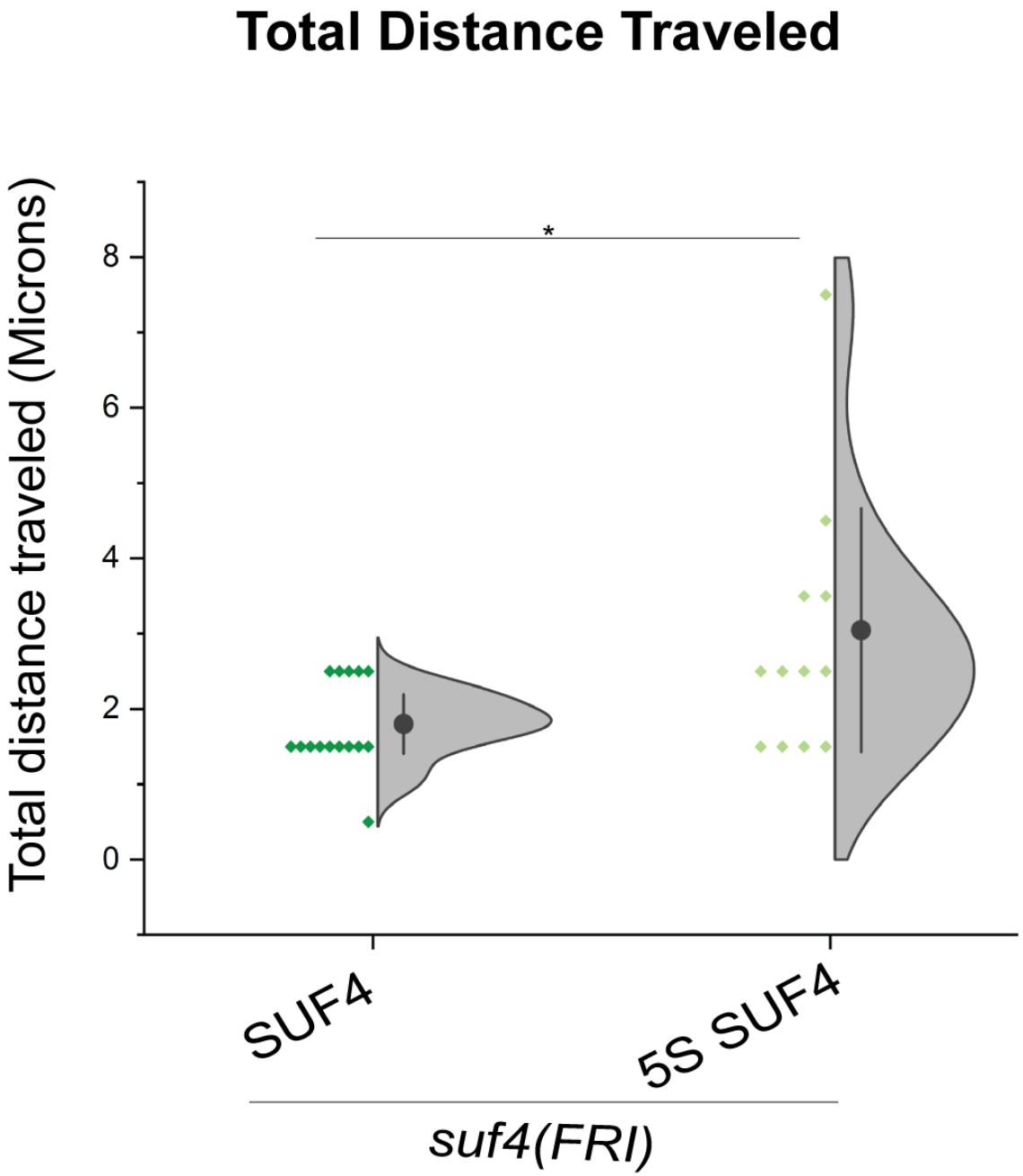

Supplemental Figure 6. Quantification of the total distance traveled for condensates used in FRAP (Figure 2F). On average 5S condensates were more mobile. Vertical line equals standard deviations. Asterisks denote P-values from Student's T- test * <0.01

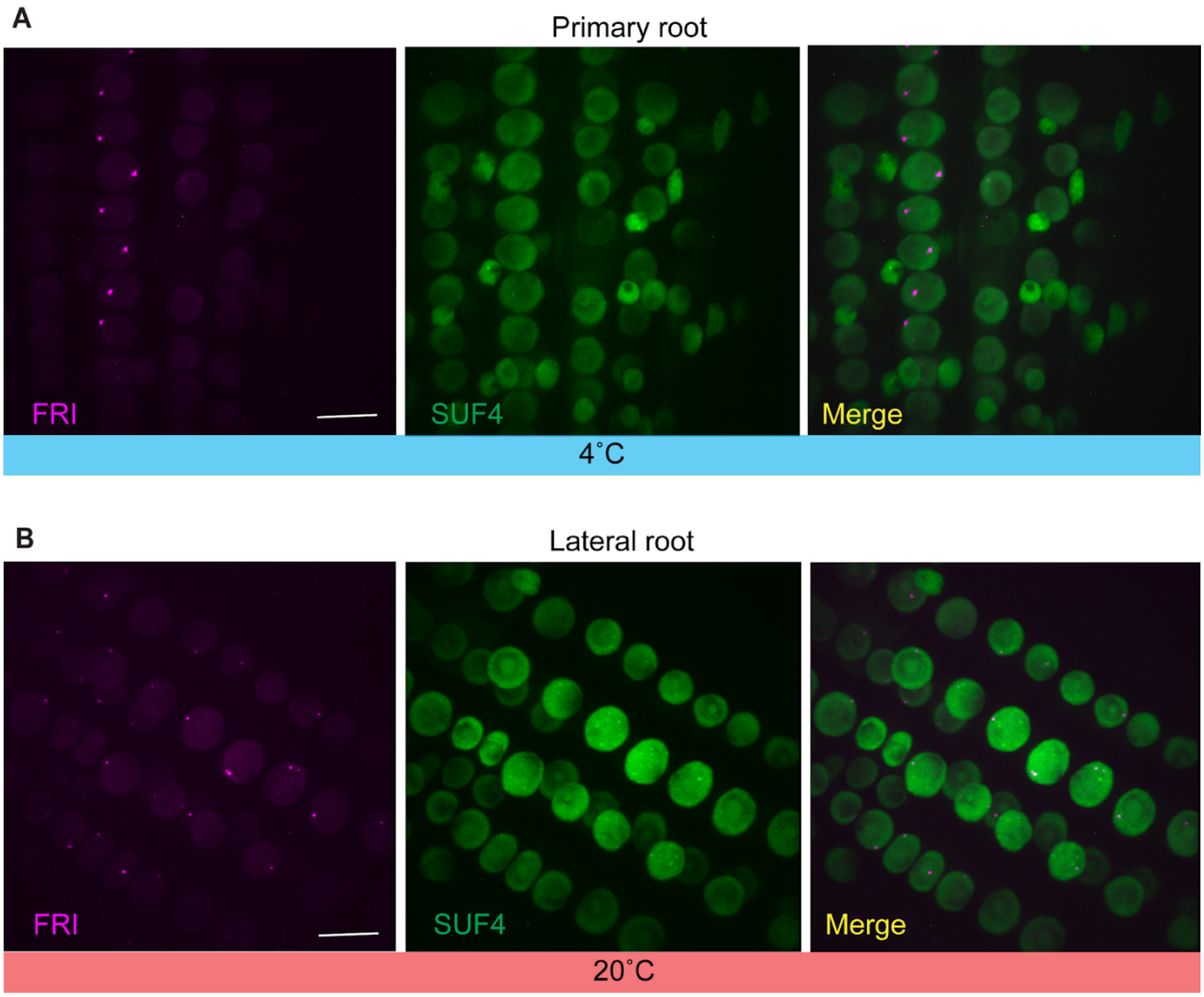

Supplemental Figure 7. A) FRI forms condensates in the primary root of 6 day old seedlings after 24 hours of 4˚C treatment. **B)** FRI forms condensates in a burst-like fashion in lateral roots under warm temperatures. Scalebar =10µm

REFERENCES:

1. C. A. Helliwell, C. C. Wood, M. Robertson, W. J. Peacock, E. S. Dennis, The Arabidopsis FLC protein interacts directly in vivo with SOC1 and FT chromatin and is part of a high-molecular-weight protein complex. *Plant J.* **46**, 183–192 (2006).

2. I. Searle, Y. He, F. Turck, C. Vincent, F. Fornara, S. Kröber, R. A. Amasino, G. Coupland, The transcription factor FLC confers a flowering response to vernalization by repressing meristem competence and systemic signaling in Arabidopsis. *Genes Dev.* **20**, 898–912 (2006).

3. K. Choi, J. Kim, H.-J. Hwang, S. Kim, C. Park, S. Y. Kim, I. Lee, The FRIGIDA complex activates transcription of FLC, a strong flowering repressor in Arabidopsis, by recruiting chromatin modification factors. *Plant cell* **23**, 289–303 (2011).

4. D.-H. Kim, S. Sung, Vernalization-Triggered Intragenic Chromatin Loop Formation by Long Noncoding RNAs. *Dev. Cell* **40**, 302-312.e4 (2017).

5. T. Csorba, J. I. Questa, Q. Sun, C. Dean, Antisense COOLAIR mediates the coordinated switching of chromatin states at FLC during vernalization. *Proc. Natl. Acad. Sci.* **111**, 16160–16165 (2014).

6. S. K. Kik, D. Christopher, H. Glauninger, C. W. Hickernell, J. A. M. Bard, M. Ford, T. R. Sosnick, D. A. Drummond, An adaptive biomolecular condensation response is conserved across environmentally divergent species. *bioRxiv*, 2023.07.28.551061 (2023).

7. D. Moses, G. M. Ginell, A. S. Holehouse, S. Sukenik, Intrinsically disordered regions are poised to act as sensors of cellular chemistry. *Trends Biochem. Sci.*, doi: 10.1016/j.tibs.2023.08.001 (2023).

8. E. W. Martin, T. Mittag, Relationship of Sequence and Phase Separation in Protein Low-Complexity Regions. *Biochemistry* **57**, 2478–2487 (2018).

9. Z. Zhang, X. Luo, Y. Yang, Y. He, Cold induction of nuclear FRIGIDA condensation in Arabidopsis. *Nature* **619**, E27–E32 (2023).

10. P. Zhu, C. Lister, C. Dean, Cold-induced Arabidopsis FRIGIDA nuclear condensates for FLC repression. *Nature* **599**, 657–661 (2021).

11. P. Zhu, C. Dean, Reply to: Cold induction of nuclear FRIGIDA condensation in Arabidopsis. *Nature* **619**, E33–E37 (2023).

12. X. Fang, L. Wang, R. Ishikawa, Y. Li, M. Fiedler, F. Liu, G. Calder, B. Rowan, D. Weigel, P. Li, C. Dean, Arabidopsis FLL2 promotes liquid–liquid phase separation of polyadenylation complexes. *Nature* **569**, 265–269 (2019).

13. Q. Zhang, K. Deng, M. Liu, S. Yang, W. Xu, T. Feng, M. Jie, Z. Liu, X. Sheng, H. Chen, H. Jiang, Phase separation of BuGZ regulates gut regeneration and aging through interaction with m6A regulators. *Nat. Commun.* **14**, 6700 (2023).

14. H. Jiang, S. Wang, Y. Huang, X. He, H. Cui, X. Zhu, Y. Zheng, Phase Transition of Spindle-Associated Protein Regulate Spindle Apparatus Assembly. *Cell* **163**, 108–122 (2015).

15. A. F. Chin, Y. Zheng, V. J. Hilser, Phylogenetic convergence of phase separation and mitotic function in the disordered protein BuGZ. *Protein Sci.* **31**, 822–834 (2022).

16. D. Stępiński, Functional ultrastructure of the plant nucleolus. *Protoplasma* **251**, 1285–1306 (2014).

17. P. J. Shaw, J. W. Brown, Plant nuclear bodies. *Curr. Opin. Plant Biol.* **7**, 614–620 (2004).

18. N. O. Kalinina, S. Makarova, A. Makhotenko, A. J. Love, M. Taliansky, The Multiple Functions of the Nucleolus in Plant Development, Disease and Stress Responses. *Front. Plant Sci.* **9**, 132 (2018).

19. R. Ietswaart, S. Rosa, Z. Wu, C. Dean, M. Howard, Cell-Size-Dependent Transcription of FLC and Its Antisense Long Non-coding RNA COOLAIR Explain Cell-to-Cell Expression Variation. *Cell Syst.* **4**, 622-635.e9 (2017).

20. S. Rosa, S. Duncan, C. Dean, Mutually exclusive sense–antisense transcription at FLC facilitates environmentally induced gene repression. *Nat. Commun.* **7**, 13031 (2016).

21. S. Kroschwald, S. Alberti, Gel or Die: Phase Separation as a Survival Strategy. *Cell* **168**, 947–948 (2017).

22. S. Alberti, The wisdom of crowds: regulating cell function through condensed states of living matter. *J. Cell Sci.* **130**, 2789–2796 (2017).

23. Z. Wang, J. Lou, H. Zhang, Essence determines phenomenon: Assaying the material properties of biological condensates. *J. Biol. Chem.* **298**, 101782 (2022).

24. J. A. Riback, C. D. Katanski, J. L. Kear-Scott, E. V. Pilipenko, A. E. Rojek, T. R. Sosnick, D. A. Drummond, Stress-Triggered Phase Separation Is an Adaptive, Evolutionarily Tuned Response. *Cell* **168**, 1028-1040.e19 (2017).

25. Y. Shin, C. P. Brangwynne, Liquid phase condensation in cell physiology and disease. *Science* **357** (2017).

26. D. S. Vazquez, P. L. Toledo, A. R. Gianotti, M. R. Ermácora, Protein conformation and biomolecular condensates. *Curr. Res. Struct. Biol.* **4**, 285–307 (2022).

27. Y. Dorone, S. Boeynaems, E. Flores, B. Jin, S. Hateley, F. Bossi, E. Lazarus, J. G. Pennington, E. Michiels, M. D. Decker, K. Vints, P. Baatsen, G. W. Bassel, M. S. Otegui, A. S. Holehouse, M. Exposito-Alonso, S. Sukenik, A. D. Gitler, S. Y. Rhee, A prion-like protein regulator of seed germination undergoes hydration-dependent phase separation. *Cell* **184**, 4284-4298.e27 (2021).

28. K. Lasker, S. Boeynaems, V. Lam, D. Scholl, E. Stainton, A. Briner, M. Jacquemyn, D. Daelemans, A. Deniz, E. Villa, A. S. Holehouse, A. D. Gitler, L. Shapiro, The material properties of a bacterial-derived biomolecular condensate tune biological function in natural and synthetic systems. *Nat. Commun.* **13**, 5643 (2022).

29. S. Y. Kim, S. D. Michaels, SUPPRESSOR OF FRI 4 encodes a nuclear-localized protein that is required for delayed flowering in winter-annual Arabidopsis. *Development* **133**, 4699–4707 (2006).

30. W. F. Beckman, M. Á. L. Jiménez, P. J. Verschure, Transcription bursting and epigenetic plasticity: an updated view. *Epigenetics Commun.* **1**, 6 (2021).

31. S. K. Powers, A. S. Holehouse, D. A. Korasick, K. H. Schreiber, N. M. Clark, H. Jing, R. Emenecker, S. Han, E. Tycksen, I. Hwang, R. Sozzani, J. M. Jez, R. V. Pappu, L. C. Strader, Nucleo-cytoplasmic Partitioning of ARF Proteins Controls Auxin Responses in Arabidopsis thaliana. *Mol. Cell* **76**, 177-190.e5 (2019).

32. Y. He, M. R. Doyle, R. M. Amasino, PAF1-complex-mediated histone methylation of FLOWERING LOCUS C chromatin is required for the vernalization-responsive, winter-annual habit in Arabidopsis. *Genes Dev.* **18**, 2774–2784 (2004).

33. K. Bugge, L. Staby, K. R. Kemplen, C. O'Shea, S. K. Bendsen, M. K. Jensen, J. G. Olsen, K. Skriver, B. B. Kragelund, Structure of Radical-Induced Cell Death1 Hub Domain Reveals a Common αα-Scaffold for Disorder in Transcriptional Networks. *Structure* **26**, 734-746.e7 (2018).

34. J. Jiang, T. Wang, Z. Wu, J. Wang, C. Zhang, H. Wang, Z.-X. Wang, X. Wang, The Intrinsically Disordered Protein BKI1 Is Essential for Inhibiting BRI1 Signaling in Plants. *Mol. Plant* **8**, 1675–1678 (2015).

35. F. Pazos, N. Pietrosemoli, J. A. García-Martín, R. Solano, Protein intrinsic disorder in plants. *Front. Plant Sci.* **4**, 363 (2013).

36. W. Deng, H. Ying, C. A. Helliwell, J. M. Taylor, W. J. Peacock, E. S. Dennis, FLOWERING LOCUS C (FLC) regulates development pathways throughout the life cycle of Arabidopsis. *Proc. Natl. Acad. Sci.* **108**, 6680–6685 (2011).

37. C. Shindo, M. J. Aranzana, C. Lister, C. Baxter, C. Nicholls, M. Nordborg, C. Dean, Role of FRIGIDA and FLOWERING LOCUS C in Determining Variation in Flowering Time of Arabidopsis. *Plant Physiol.* **138**, 1163–1173 (2005).

38. S. Roberts, T. S. Harmon, J. L. Schaal, V. Miao, K. (Jonathan) Li, A. Hunt, Y. Wen, T. G. Oas, J. H. Collier, R. V. Pappu, A. Chilkoti, Injectable tissue integrating networks from recombinant polypeptides with tunable order. *Nat. Mater.* **17**, 1154–1163 (2018).

39. F. G. Quiroz, A. Chilkoti, Sequence heuristics to encode phase behaviour in intrinsically disordered protein polymers. *Nat. Mater.* **14**, 1164–1171 (2015).

40. K. M. Ruff, S. Roberts, A. Chilkoti, R. V. Pappu, Advances in Understanding Stimulus-Responsive Phase Behavior of Intrinsically Disordered Protein Polymers. *J. Mol. Biol.* **430**, 4619–4635 (2018).

41. M. Dzuricky, B. A. Rogers, A. Shahid, P. S. Cremer, A. Chilkoti, De novo engineering of intracellular condensates using artificial disordered proteins. *Nat. Chem.* **12**, 814–825 (2020).

42. J. W. Chen, P. Romero, V. N. Uversky, A. K. Dunker, Conservation of Intrinsic Disorder in Protein Domains and Families: I. A Database of Conserved Predicted Disordered Regions. *J. Proteome Res.* **5**, 879–887 (2006).

43. A. C. Riley, D. A. Ashlock, S. P. Graether, The difficulty of aligning intrinsically disordered protein sequences as assessed by conservation and phylogeny. *PLOS ONE* **18**, e0288388 (2023).

44. Y. Wan, X. Zheng, H. Chen, Y. Guo, H. Jiang, X. He, X. Zhu, Y. Zheng, Splicing function of mitotic regulators links R-loop–mediated DNA damage to tumor cell killing. *J. Cell Biol.* **209**, 235–246 (2015).

45. Z. Bao, N. Zhang, J. Hua, Endopolyploidization and flowering time are antagonistically regulated by checkpoint component MAD1 and immunity modulator MOS1. *Nat. Commun.* **5**, 5628 (2014).

46. F. Resentini, P. Cyprys, J. G. Steffen, S. Alter, P. Morandini, C. Mizzotti, A. Lloyd, G. N. Drews, T. Dresselhaus, L. Colombo, S. Sprunck, S. Masiero, SUPPRESSOR OF FRIGIDA (SUF4) Supports Gamete Fusion via Regulating Arabidopsis EC1 Gene Expression. *Plant Physiol.* **173**, 155–166 (2016).

47. J. V. Leene, J. Hollunder, D. Eeckhout, G. Persiau, E. V. D. Slijke, H. Stals, G. V. Isterdael, A. Verkest, S. Neirynck, Y. Buffel, S. D. Bodt, S. Maere, K. Laukens, A.

Pharazyn, P. C. G. Ferreira, N. Eloy, C. Renne, C. Meyer, J. Faure, J. Steinbrenner, J. Beynon, J. C. Larkin, Y. V. de Peer, P. Hilson, M. Kuiper, L. D. Veylder, H. V. Onckelen, D. Inzé, E. Witters, G. D. Jaeger, Targeted interactomics reveals a complex core cell cycle machinery in Arabidopsis thaliana. *Mol. Syst. Biol.* **6**, 397–397 (2010).

48. I. Lee, R. M. Amasino, Effect of Vernalization, Photoperiod, and Light Quality on the Flowering Phenotype of Arabidopsis Plants Containing the FRIGIDA Gene. *Plant Physiol.* **108**, 157–162 (1995).

49. J. Schindelin, I. Arganda-Carreras, E. Frise, V. Kaynig, M. Longair, T. Pietzsch, S. Preibisch, C. Rueden, S. Saalfeld, B. Schmid, J.-Y. Tinevez, D. J. White, V. Hartenstein, K. Eliceiri, P. Tomancak, A. Cardona, Fiji: an open-source platform for biological-image analysis. *Nat. Methods* **9**, 676–682 (2012).

50. D. Ershov, M.-S. Phan, J. W. Pylvänäinen, S. U. Rigaud, L. L. Blanc, A. Charles-Orszag, J. R. W. Conway, R. F. Laine, N. H. Roy, D. Bonazzi, G. Duménil, G. Jacquemet, J.-Y. Tinevez, TrackMate 7: integrating state-of-the-art segmentation algorithms into tracking pipelines. *Nat. methods* **19**, 829–832 (2021).

51. G. Koulouras, A. Panagopoulos, M. A. Rapsomaniki, N. N. Giakoumakis, S. Taraviras, Z. Lygerou, EasyFRAP-web: a web-based tool for the analysis of fluorescence recovery after photobleaching data. *Nucleic Acids Res.* **46**, W467–W472 (2018).